Supporting Information

Selective oxidation of aliphatic C-H bonds in alkylphenols by a chemomimetic biocatalytic system

Lei Du[a,b,c,1], Sheng Dong[a,b,1], Xingwang Zhang[a,b], Chengying Jiang[d,e], Jingfei Chen[a,b], Lishan Yao[a,b], Xiao Wang[f], Xiaobo Wan[f], Xi Liu[g,h,i], Xinquan Wang[g,h,i], Shaohua Huang[a,b], Qiu Cui[a,b], Yingang Feng[a,b,2], Shuang-Jiang Liu[d,e,2], and Shengying Li[a,b,2]

[a]Shandong Provincial Key Laboratory of Synthetic Biology, Qingdao Institute of Bioenergy and Bioprocess Technology, Chinese Academy of Sciences, Qingdao, Shandong 266101, China; [b]Key Laboratory of Biofuels, Qingdao Institute of Bioenergy and Bioprocess Technology, Chinese Academy of Sciences, Qingdao, Shandong 266101, China; [c]University of Chinese Academy of Sciences, Beijing 100049, China; [d]State Key Laboratory of Microbial Resources, Institute of Microbiology, Chinese Academy of Sciences, Beijing 100101, China; [e]Environmental Microbiology and Biotechnology Research Center, Institute of Microbiology, Chinese Academy of Sciences, Beijing 100101, China; [f]Key Laboratory of Bio-based Materials, Qingdao Institute of Bioenergy and Bioprocess Technology, Chinese Academy of Sciences, Qingdao, Shandong 266101, China; [g]Ministry of Education Key Laboratory of Protein Science, School of Life Sciences, Tsinghua University, Beijing 100084, China; [h]Beijing Advanced Innovation Center for Structural Biology, School of Life Sciences, Tsinghua University, Beijing 100084, China; and [i]Collaborative Innovation Center for Biotherapy, School of Life Sciences, Tsinghua University, Beijing 100084, China

[1]L.D. and S.D. contributed equally to this work.

[2]To whom correspondence should be addressed. E-mail: fengyg@qibebt.ac.cn (Y. Feng), liusj@im.ac.cn (S.-J. Liu), and lishengying@qibebt.ac.cn (S. Li)

Table of Contents

SI Methods

Strains and culture conditions. The bacterial strains and plasmids used in this study are listed in Table S3. *Escherichia coli* strains were grown at 37 °C on LB agar (2% w/v) plates or LB liquid broth. *E. coli* DH5α strain was used for vector construction and plasmid isolation. For protein expression and purification, *E. coli* BL21 (DE3) strain was cultured in Terrific Broth (TB) medium (1) with a rotary shaker (220 rpm). When required, kanamycin was added to a final concentration of 50 μg/ml.

DNA isolation and manipulation. Plasmids were isolated using the E.Z.N.A.^{TM} Plasmid Miniprep Kit (Omega Biotek, Norcross, GA). DNA fragments were purified using the Wizard SV Gel and PCR Clean-up System (Promega, Madison, USA). Vector transformation, agarose gel electrophoresis and other standard techniques of molecular cloning were performed as previously described (2).

General protein expression, purification and concentration determination. For protein expression, *E. coli* BL21 (DE3) carrying a specific expression vector was grown in LB broth containing 50 μg/ml kanamycin at 37 °C overnight. Terrific Broth (1 l) supplemented with 4% glycerol was inoculated with a 1:100 dilution of the overnight culture. The culture was then incubated on a rotary shaker (220 rpm) at 37 °C until the OD_{600} reached ~0.6. Next, IPTG (final concentration of 0.2 mM) was added into the culture to induce protein expression. Cultivation continued for additional 20 h at 18 °C.

Protein purification was carried out as described elsewhere (3) with minor modifications. All procedures were performed at 4 °C. The cells were harvested by centrifugation (5000 × *g* for 5 min), washed with deionized water for 2 times, and re-suspended in 50 ml of lysis buffer (50 mM NaH_2PO_4, 300 mM NaCl, 10% glycerol and 10 mM imidazole, pH 8.0). After sonication on ice, the crude cell lysate was centrifuged at 12,000 ×*g* for 30 min to collect the supernatant fraction. Subsequently, 1 ml of Ni-NTA resin (Qiagen, Germany) was added into the supernatant with subsequent incubation at 4 °C on a gentle rotator for 30 min. This slurry was loaded onto an empty column, and washed with ~100 ml wash buffer (50 mM NaH_2PO_4, 300 mM NaCl, 10% glycerol and 20 mM imidazole, pH 8.0) until no proteins were detectable in flow-through by Coomassie Brilliant Blue G-250 assays. Approximately 10 ml of elution buffer (50 mM NaH_2PO_4, 300 mM NaCl, 10% glycerol and 250 mM imidazole, pH 8.0) was

used to elute target proteins from the Ni-NTA resin. The eluent was concentrated with an Amicon Ultra centrifugal filter (Merck KGaA, Darmstadt, Germany) (7500 × *g* for 30 min) and buffer exchanged on a PD-10 column (GE Healthcare, Buckinghamshire, UK) with 5 ml desalting buffer (50 mM NaH_2PO_4, 10% glycerol, pH 7.5). The desalted enzyme solution was again concentrated to about 1 ml using Amicon Ultra centrifugal filter. The protein aliquots were flash frozen by liquid nitrogen and stored at -80 °C.

Concentrations of non-P450 enzymes (CreH, CreI, CreE, CreF, CreD, CreG and CreC) were determined by the Bradford method using BSA as the standard (4). The concentration of P450 enzymes (wt and mutant CreJ enzymes) was determined according to the method described by Omura (5). Specifically, the CO-bound reduced difference spectrum was recorded by NanoDrop 2000 Spectrophotometer (Thermo Scientific). The concentration of functional P450 was calculated using the extinction coefficient ($\epsilon_{450\ nm–490\ nm}$) of 91000 $M^{-1}\cdot cm^{-1}$.

Expression and purification of CreJ for crystallization procedures. To facilitate heterologous expression of CreJ*,* the *creJ* gene with the first 84 nucleotides truncated was cloned into pET28a between *Bam*HI and *Hind*III restriction sites. The shortened protein containing an *N*-terminal His_6-tag was expressed in *Escherichia coli* BL21 (DE3) and purified using a Ni^{2+} Sepharose HP column (GE healthcare). The protein was further purified by anion exchange chromatography with a Q-sepharose column (GE healthcare) and gel filtration using a Superdex 75 column (GE healthcare). The gel filtration result indicates that the recombinant CreJ is monomeric in solution.

CreJ mutagenesis and relative activity determination. Mutation sites were introduced via PCR (Table S4). Specifically, complimentary primer pairs containing the mutated codon of interest were employed in PCR amplifications (35 cycles of 95 °C for 10 s, 55 °C for 15 s, and 72 °C for 2 min; FailSafe system from Epicentre) to yield a linear mutant plasmid from the original pET28a-*creJ* template DNA. Following gel purification, each linear mutant plasmid was treated with homologous recombinase (Hieff Clone TM One Step Cloning Kit, Yeasen, Shanghai, China) following vendor's protocols, followed by transformation into *E. coli* BL21(DE3). The incorporation of the mutated codon was confirmed via Sanger DNA sequencing (GENEWIZ, Suzhou, China).

Wild-type and mutant enzymatic activities were comparatively determined in reactions using **1'** as substrate, at 30 °C for 20 min. A standard reaction mixture contained 1 μM CreJ (or CreJ mutant), 1 μM CreE and 1 μM CreF, 1 mM substrate, and 4 mM NADPH in 100 μl of 50 mM Tris·HCl (pH 8.0). The substrate consumption ratio of each reaction was determined by high-performance liquid chromatography (HPLC). Relative enzymatic activity of each mutant was calculated by comparing substrate consumption ratios to that of CreJ, which was assigned 100% activity. All reactions were carried out in triplicate and the data was reported as the means ± SD.

Substrate binding assays. Spectroscopic substrate binding assays were carried out at room temperature by employing a UV visible spectrophotometer (Infinite M200 pro, TECAN) (6). Protein dissolved in 1 mL of 50 mM sodium phosphate buffer containing 10% glycerol (pH 7.4) at concentration of 1 μM was titrated with 100 mM stock solution of 4-cresol. The final concentration of substrate ranged from 0.2 to 0.8 mM. Data consisting of absorbance differences ΔA ($A_{390\ nm}$ - $A_{420\ nm}$) and corresponding substrate concentration from duplicated experiments were plotted and fitted to the hyperbolic function $\Delta A = A_{max} \cdot S/(K_D + S)$, where S is the total substrate concentration, A_{max} is the maximal absorption shift at saturation, and K_D is the apparent dissociation constant for the enzyme-substrate complex.

Chiral HPLC analysis of 2a and 7a. The reaction sample was extracted with an equal volume of ethyl acetate. The organic phase was dried by nitrogen stream and re-constituted in an equal volume of methanol. The chiral column (250 × 4.6 mm) was manually packed with the chiral stationary phase, which was prepared by coating chitosan bis(3-chlorophenylcarbamate)-(cyclohexyl urea) on the surface of 3-aminopropyl silica gel according to a previously published method (7).

Chiral analysis was carried out on an Agilent 1260 infinity HPLC system (Agilent Technologies, USA) equipped with a DAD detector. The two enantiomers of **2a** and **7a** were respectively separated on the chiral column described above using an isocratic mobile phase of hexane containing 10% isopropanol over 60 min. The flow rate was set to 1 ml/min and injection volume was 10 μl. The detection wavelength was set to 275 nm. Optical configuration was determined via retention time comparison with the enantiomerically pure authentic standard.

Sources of substrates and authentic standard compounds. Except the phosphorylated compounds that were chemically synthesized (*see below*), all substrates and authentic standard compounds were purchased from different chemical suppliers. In details, **2** was bought from Tokyo Chemical Industry (TCI, Shanghai, China); **3**, **4b**, **6a**, **7b**, **11** and **12** from J&K Scientific Ltd. (Beijing, China); **4** from Acros Organics (Thermo Fisher Scientific, USA); **5**, **6** and **9** from AIKE REAGENT (Chengdu, China); **7** from Sigma-Aldrich (USA), **8** from Toronto Research Chemicals (TRC, Canada); **10** from Fluorochem (Derbyshire, UK), **5b** and racemic **2a** from Bide Pharmatech Ltd. (Shanghai, China); **5a** and the enantiomerically pure *S*-**2a** and *S*-**7a** from Enamine (Ukraine); **2b**, **3b**, **6b** and **6c** from Aladdin (Shanghai, China); racemic **7a** from Accela ChemBio (San Diego, CA, USA). **1'** was synthesized by following the chemical method with reference to the previous report (8).

Chemical synthesis of 4-ethylphenyl phosphate (2'). Compound **2'** was synthesized through chemical methods with reference to previous reports by McKenna and Kenner (9, 10). The reaction scheme is as follow:

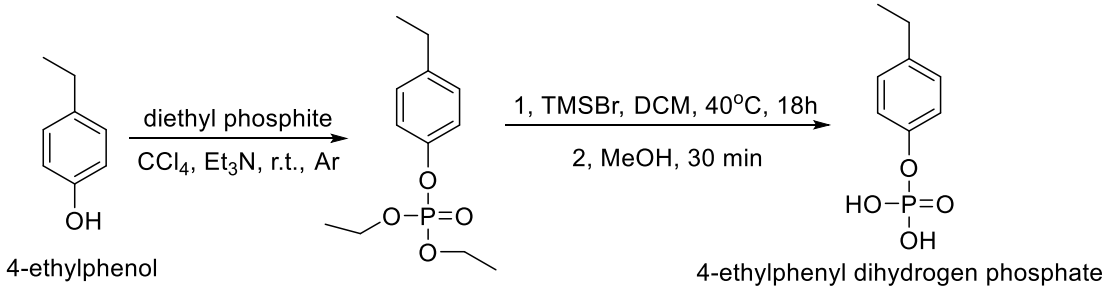

In details, to a solution of 4-ethylphenol (1.22 g, 10 mmol) dissolved in carbon tetrachloride (10 mL) was added diethyl phosphite (1.55 mL, 12 mmol) at 0 °C under argon atmosphere. Triethylamine (1.65 mL, 12 mmol) was carefully added drop-wise to the mixture by using a dropping funnel. The mixture was stirred overnight at room temperature. Water (30 mL) was added and the organic layer was separated. The organic layer was washed twice with dilute hydrochloric acid (2 × 15 mL), four times with dilute sodium hydroxide solution (4 × 15 mL), and twice with brine (2 × 15 mL) before being dried over anhydrous $MgSO_4$. Removal of solvent on rotary evaporator gave a crude, which was further purified by silica gel column chromatography using a petroleum ether/ethyl acetate (4/1: v/v) mixture to afford diethyl (4-ethylphenyl) phosphate (2.51 g). Yield: 97 %.

Diethyl (4-ethylphenyl) phosphate (2.51 g, 9.7 mmol) was dissolved in dry CH_2Cl_2 (50 mL). Then bromotrimethylsilane (12.8 mL, 10 equiv. to phosphate ester) was added to the solution and the mixture was heated to reflux for 18 h under argon atmosphere. The solvent was evaporated and the residue was dissolved in anhydrous methanol (50 mL). The solution was stirred for 30 min at 40 °C. Then the resulting solution was concentrated to give **2'** (1.8 g). Yield: 92%. Structure of synthetic **2'** was confirmed by HRMS (Fig. S42) and NMR (Fig. S43 and S44).

Chemical synthesis of 1-hexanol phosphate (11') and 4-methyl cyclohexanol phosphate (12'). Compound **11'** was chemically synthesized using previously reported methods (11). The reaction scheme is as follow:

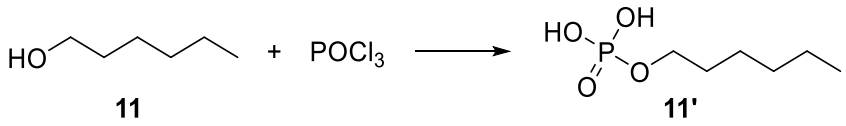

In details, **11'** was prepared by mixing **11** (5 mmol, 0.51 g) with the reagent phosphorus oxychloride (5 mmol, 0.77 g), by vigorous stirring for 1 h under aspirator vacuum to remove HCl (g), and then heated at 50 °C for 5 h. The reaction was quenched via a dropwise addition of the reaction mixture into excess cold water, and the resultant mixture was then stirred for 5 h at 30 °C. The product was extracted with Et_2O multiple times. The combined extracts were dried with anhydrous $MgSO_4$, and Et_2O was removed under reduced pressure to afford a colorless oil 0.75 g (yield: 91 %).

Compound **12'** was accessed by following previously described methods (12). The reaction scheme is as follow:

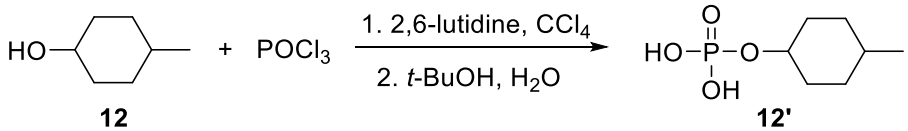

Specifically, **12** (5 mmol, 0.57 g) and 2,6-lutidine (5.5 mmol, 0.59 g) in carbon tetrachloride (2 ml) were added to phosphorous oxychloride (5mmol, 0.77 g) in carbon tetrachloride (10 ml) at 0-10 °C. After an hour, the product was filtered from base hydrochloride and evaporated, yielding the dichloridate as a colorless oil. 4-Methyl cyclohexy1 phosphorodichloridate in carbon tetrachloride (5 ml) was treated with *tert*-butyl

alcohol (0.85 g) and water (0.1 ml) for 30 min at 50 °C**.** Removal of the solvent left an oil which was dissolved in 30 ml water, and extracted with Et_2O several times. The combined extracts were dried with anhydrous $MgSO_4$, and Et_2O was removed *en vacuo* to give 0.3 g of a white solid (yield: 31 %). The chemical structures of synthetic **11'** and **12'** were confirmed by HRMS (Fig. S29 and S30) and NMR (Fig. S45-S48).

SI Tables

Table S1. Data collection and refinement statistics for CreJ structures.

Parameter	CreJ-**1'**	CreJ-**2'**
Data collection [a]		
Space group	C 1 2 1	P 43 21 2
a,b,c (Å)	125.54, 121.14, 125.61	86.07, 86.07, 125.04
α，β，γ	90.0, 90.96, 90.0	90.0, 90.0, 90.0
Wavelength	0.979	0.979
Resolution (Å)	34.56-2.0 (2.03-2.0)	35.45-1.70 (1.73-1.70)
Total reflections	454625 (17470)	687298 (36247)
Unique reflections	125653 (5928)	52282 (2731)
Completeness (%)	99.3 (94.4)	99.8 (100.0)
Multiplicity	3.6 (2.9)	13.1 (13.3)
Mean I/sigma (I)	8.5 (2.1)	20.1 (5.6)
R_{merge} [b]	0.106 (0.516)	0.091 (0.505)
Refinement		
R_{work}/R_{free} (%)	16.08/19.79	18.15/20.88
No. atoms		
Protein	12765	3252
Ligands	255	56
water	1825	552
B-factors		
Average B-factor	34.00	24.20
Proteins	33.70	22.40
Ligands	23.80	11.20
Solvent	38.10	35.80
r.m.s.d.		
Bond length (Å)	0.01	0.006
Bond angles	1.22	1.15
Ramachandran statistics		
Favored (%)	97	97
Outliers (%)	0.06	0

[a] Numbers in parentheses refer to data in the highest-resolution shell.

[b] $R_{merge}=\Sigma_{hkl}\Sigma_i|I(hkl)_i-\langle I(hkl)\rangle|/\Sigma_{hkl}\Sigma_i\langle I(hkl)_i\rangle$, where I is the observedintensity, $\langle I(hkl)\rangle$ represents the average intensity, and $I(hkl)_i$ represents the observedintensity of each unique reflection.

Table S2. Reactivity of CreHI, CreJEF and CreD towards different alkylphenols (1-10).

Alkylphenol	CreHI[a]	CreHI + CreJEF[b]	CreHI + CreJEF + CreD[c]
p-cresol (**1**)	+	+	+
p-ethylphenol (**2**)	+	+	+
p-vinylphenol (**3**)	+	+	+
p-propylphenol (**4**)	+	+	+
p-isopropylphenol (**5**)	+	+	+
m-cresol (**6**)	+	+	+
m-ethylphenol (**7**)	+	+	+
m-vinylphenol (**8**)	+	-	+
o-cresol (**9**)	+	-	+
o-ethylphenol (**10**)	-	-	-

[a]Each alkylphenol (1 mM) was phosphorylated by CreHI (10 μM for each enzyme), in the presence of 20 mM $MgCl_2$, 2 mM $MnCl_2$, and 2 mM ATP, at 30 °C for 2 h;

[b]Following the first stage of phosphorylation by CreHI[a], CreJEF (10 μM for each protein) and 2 mM NADPH were added at 30 °C for 2 h;

[c]Following the reactions catalyzed by CreHI[a] and CreJEF[b], CreD (10 μM) was added at 30 °C for 2 h;

"+" represents that substrate consumption or product formation was detected;

"-" represents neither substrate consumption nor product formation was detected.

Table S3. Strains and plasmids used in this study.

Strain, plasmid	Genotype/Phenotype	Source
E. coli BL21(DE3)		Novagen
E. coli DH5α		Invitrogen
pET28b	Expression vector	Novagen
pET28b-*creC*	Expression vector of CreC	Du L, *et al.*, 2016
pET28a-*creD*	Expression vector of CreD	Li T, *et al.*, 2014
pET28a-*creE*	Expression vector of CreE	Li T, *et al.*, 2014
pET28a-*creF*	Expression vector of CreF	Du L, *et al.*, 2016
pET28a-*creG*	Expression vector of CreG	Li T, *et al.*, 2014
pET28b-*creH*	Expression vector of CreH	Du L, *et al.*, 2016
pET28b-*creI*	Expression vector of CreI	Du L, *et al.*, 2016
pET28a-*creJ*	Expression vector of CreJ	Li T, *et al.*, 2014
pET28a-*creJ*-Q83A	Expression vector of CreJ-mutant (Q83A)	Present study
pET28a-*creJ*-S106A	Expression vector of CreJ-mutant (S106A)	Present study
pET28a-*creJ*-S109A	Expression vector of CreJ-mutant (S109A)	Present study
pET28a-*creJ*-R194A	Expression vector of CreJ-mutant (R194A)	Present study
pET28a-*creJ*-R194K	Expression vector of CreJ-mutant (R194K)	Present study
pET28a-*creJ*-R194E	Expression vector of CreJ-mutant (R194E)	Present study
pET28a-*creJ*-S261A	Expression vector of CreJ-mutant (S261A)	Present study
pET28a-*creJ*-W199A	Expression vector of CreJ-mutant (W199A)	Present study
pET28a-*creJ*-F264A	Expression vector of CreJ-mutant (F264A)	Present study
pET28a-*creJ*-I312A	Expression vector of CreJ-mutant (I312A)	Present study
pET28a-*creJ*-W315A	Expression vector of CreJ-mutant (W315A)	Present study
pET28a-*creJ*-F416A	Expression vector of CreJ-mutant (F416A)	Present study

Table S4. Primers used for mutagenesis of CreJ.

Mutant	Primer	Sequence
Q83A	Q83A-F	AAATGCA**GCA**GCCCCAGTCCGCAAG
	Q83A-R	CTGGGGC**TGC**TGCATTTTCAGAGGA
S106A	S106A-F	TGCATAC**GCA**GGATTATCAGCTCGT
	S106A-R	ATAATCC**TGC**GTATGCAGTGAAGCC
S109A	S109A-F	CGGATTA**GCA**GCTCGTATTCCACCA
	S109A-R	TACGAGC**TGC**TAATCCGGAGTATGC
R194A	R194A-F	AGATTCC**GCA**GCGGCCATGACCTGG
	R194A-R	TGGCCGC**TGC**GGAATCTGACCACCG
R194K	R194K-F	AGATTCC**AAA**GCGGCCATGACCTGG
	R194K-R	TGGCCGC**TTT**GGAATCTGACCACCG
R194E	R194E-F	AGATTCC**GAA**GCGGCCATGACCTGG
	R194E-R	TGGCCGC**TTC**GGAATCTGACCACCG
S261A	S261A-F	GCTGTAC**GCA**CTGCTTTTTGCGGGG
	S261A-R	AAAGCAG**TGC**GTACAGCAAAGAAGC
W199A	W199A-F	CATGACC**GCA**GGCGATCTTAGTGAT
	W199A-R	GATCGCC**TGC**GGTCATGGCCGCACG
F264A	F264A-F	CCTGCTT**GCA**GCGGGGCACGAAACA
	F264A-R	GCCCCGC**TGC**AAGCAGGGAGTACAG
I312A	I312A-F	CGGCTCG**GCA**GTGGGGTGGCGTCGA
	I312A-R	ACCCCAC**TGC**CGAGCCGGAGTACCG
W315A	W315A-F	CGTGGGG**GCA**CGTCGAAAAGCATTA
	W315A-R	TTCGACG**TGC**CCCCACGATCGAGCC
F416A	F416A-F	CCTCTCC**GCA**CGCGTCCCCACTTCT
	F416A-R	GGACGCG**TGC**GGAGAGGTTCTCCCG

Nucleotides in bold represent the mutated codons.

SI Figures

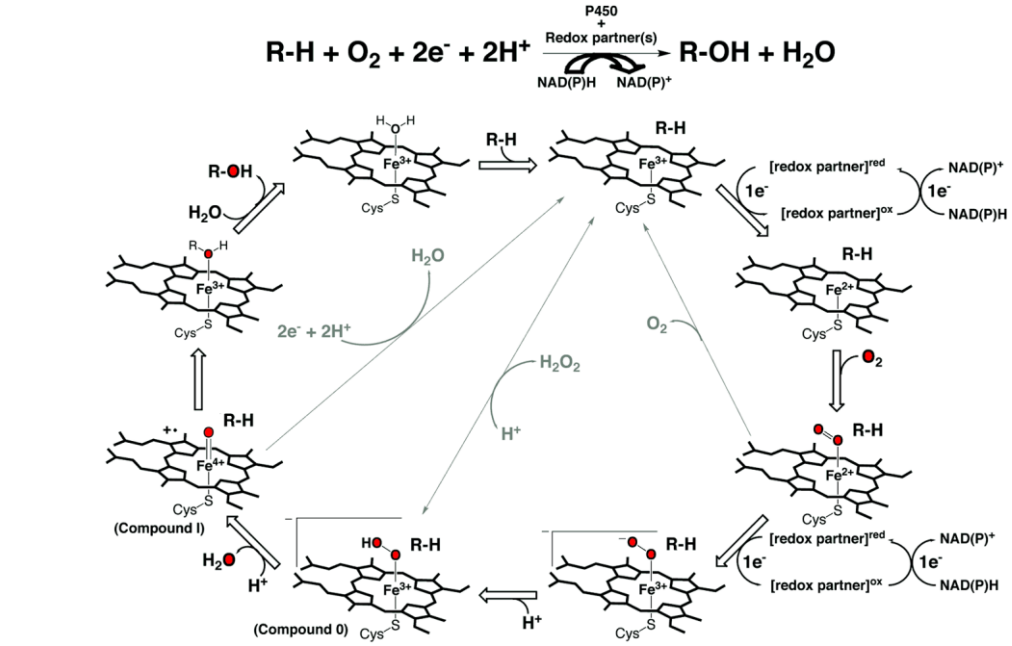

Fig. S1. The P450 catalytic cycle. (Adapted from the previous publication (13))

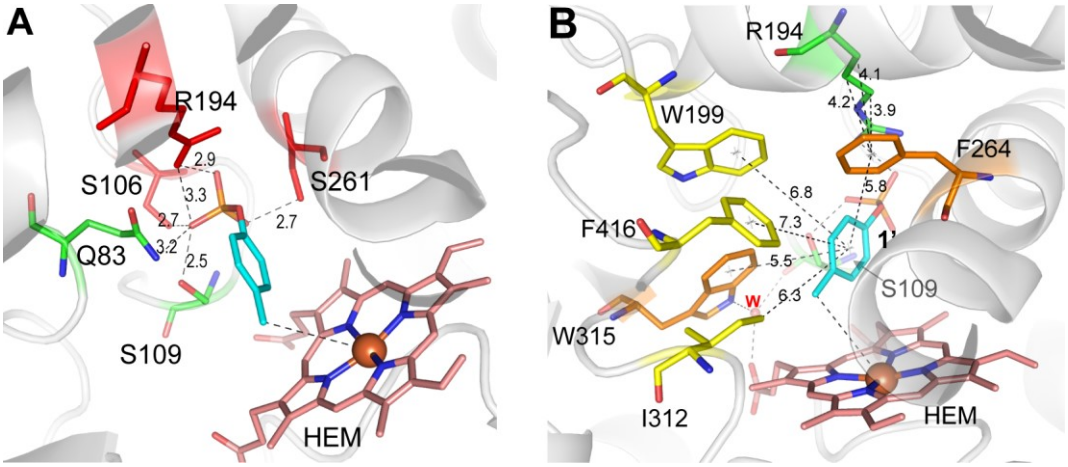

Fig. S2. Steric positions of the residues interacting with the phosphate group (*A*) and benzyl moiety (*B*) of 4-cresol.

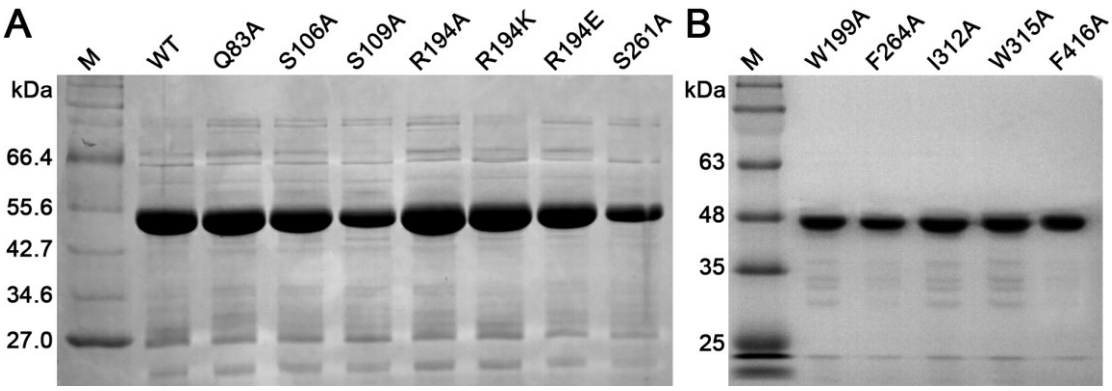

Fig. S3. SDS-PAGE analysis of purified wild-type and mutant CreJ enzymes. (*A*) Mutants of the residues interacting with the phosphate group of substrate. (*B*) Mutants of the residues surrounding the benzyl moiety of substrate. M, protein marker.

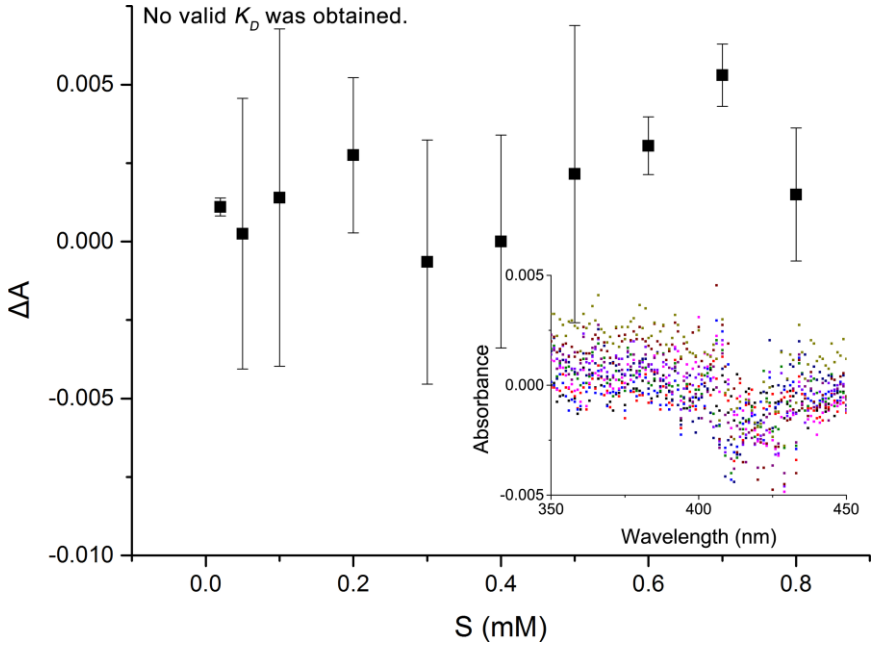

Fig. S4. The binding curve of 4-cresol to the R194A mutant.

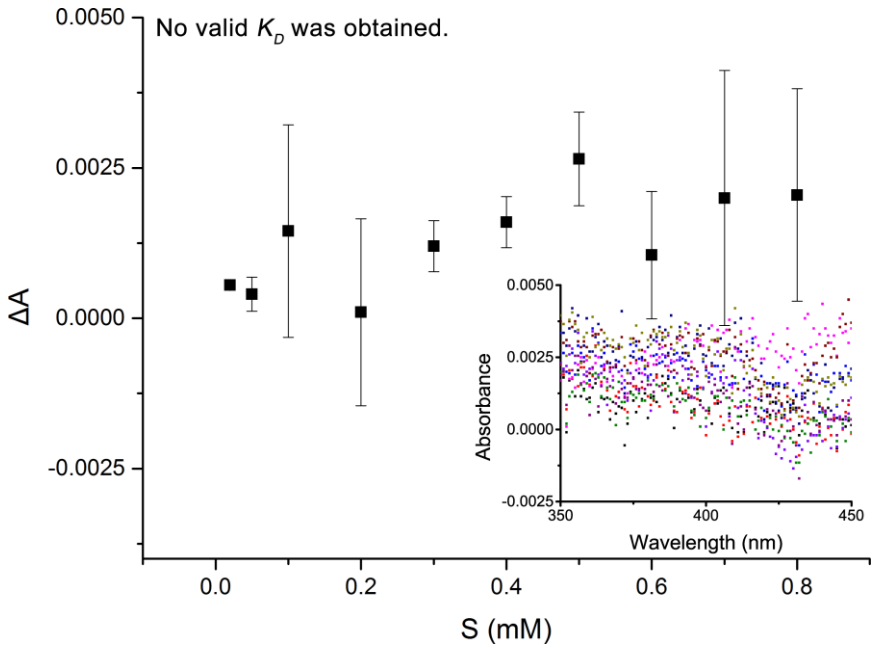

Fig. S5. The binding curve of 4-cresol to the R194K mutant.

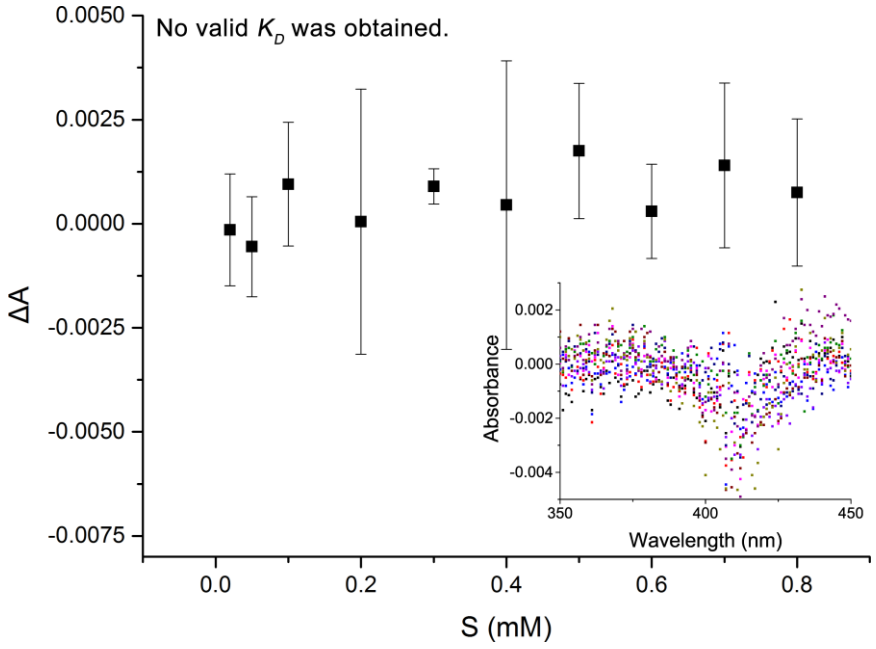

Fig. S6. The binding curve of 4-cresol to the R194E mutant.

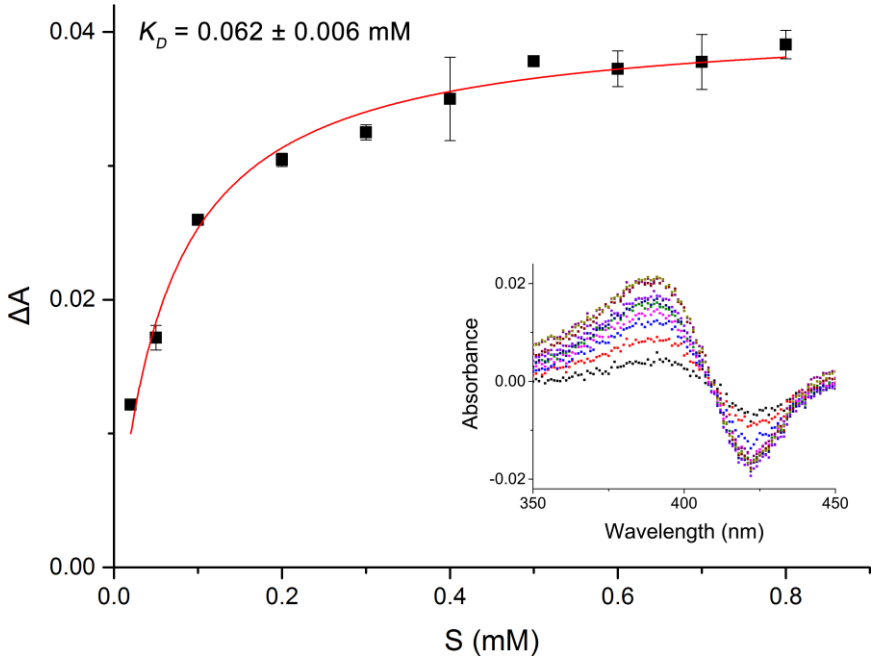

Fig. S7. The binding curve of 4-cresol to wild-type CreJ.

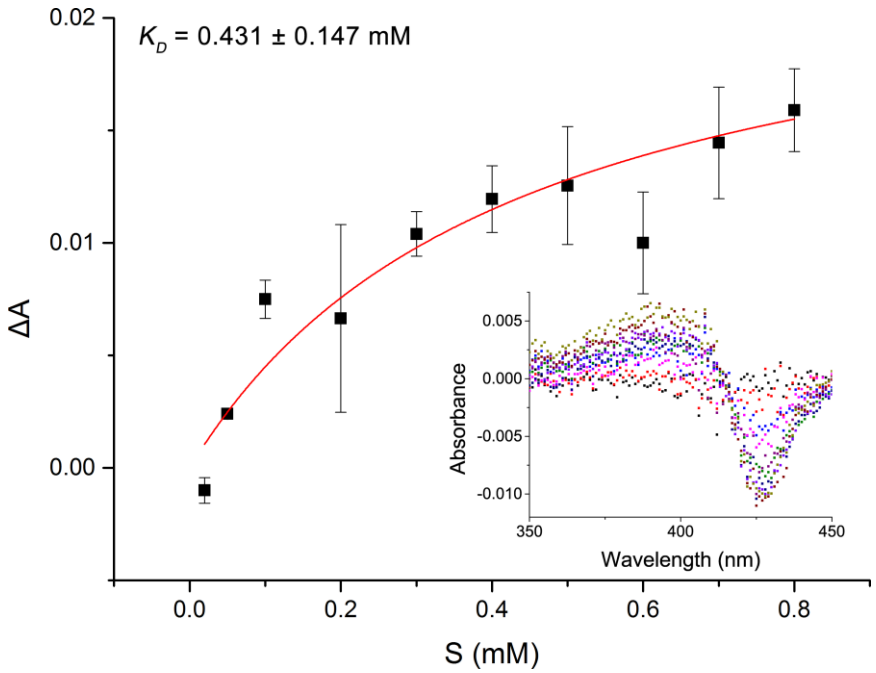

Fig. S8. The binding curve of 4-cresol to the S106A mutant.

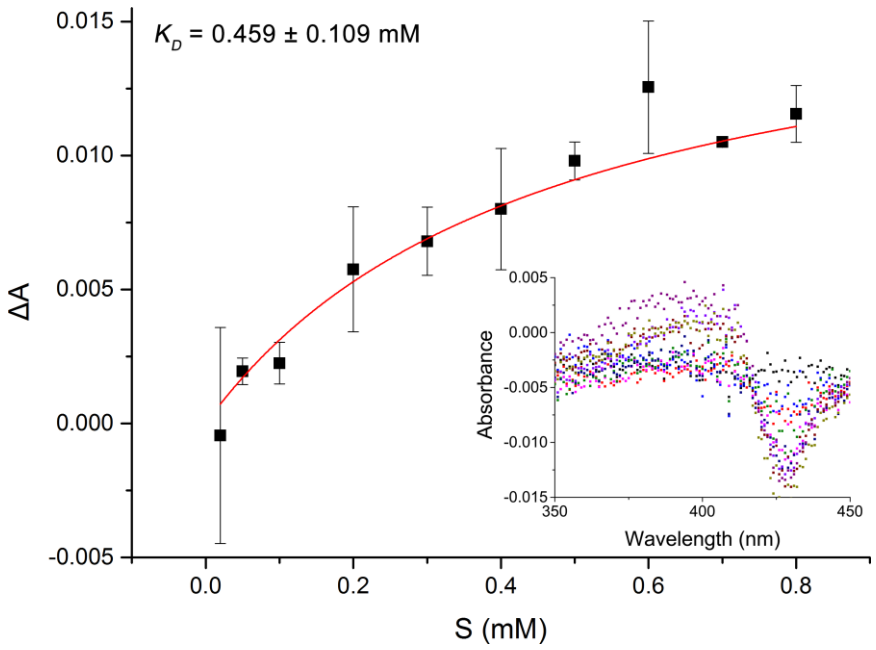

Fig. S9. The binding curve of 4-cresol to the S261A mutant.

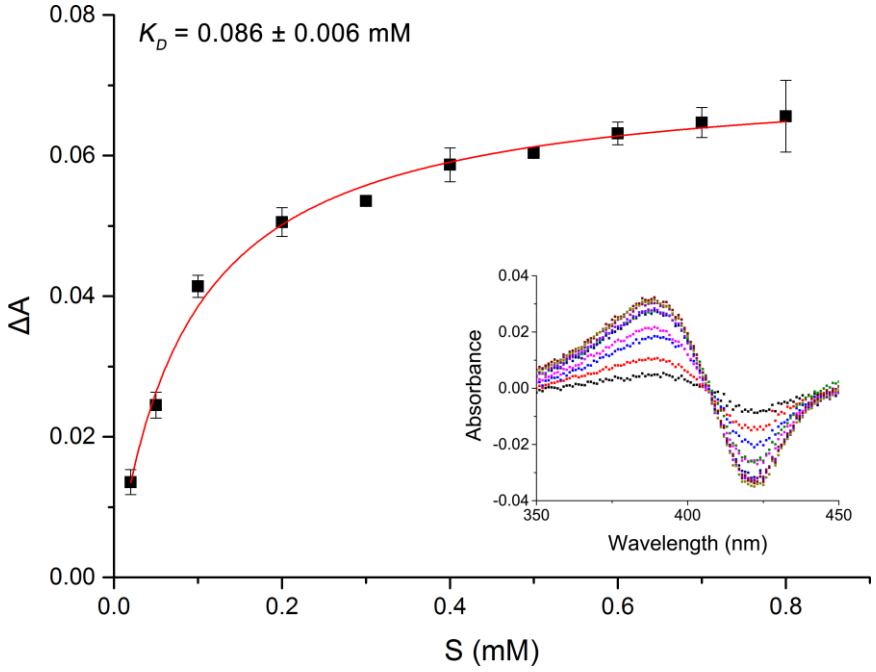

Fig. S10. The binding curve of 4-cresol to the Q83A mutant.

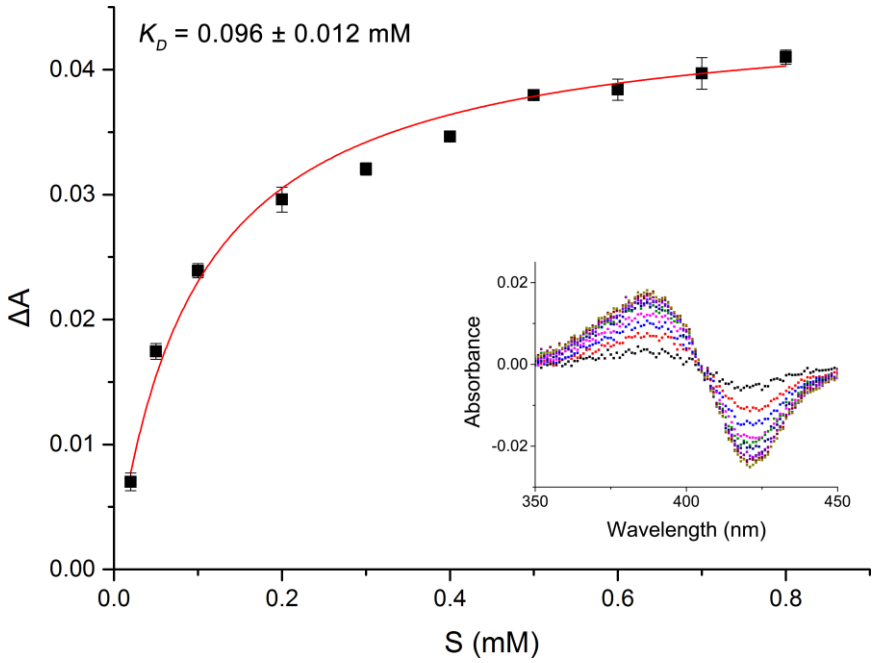

Fig. S11. The binding curve of 4-cresol to the S109A mutant.

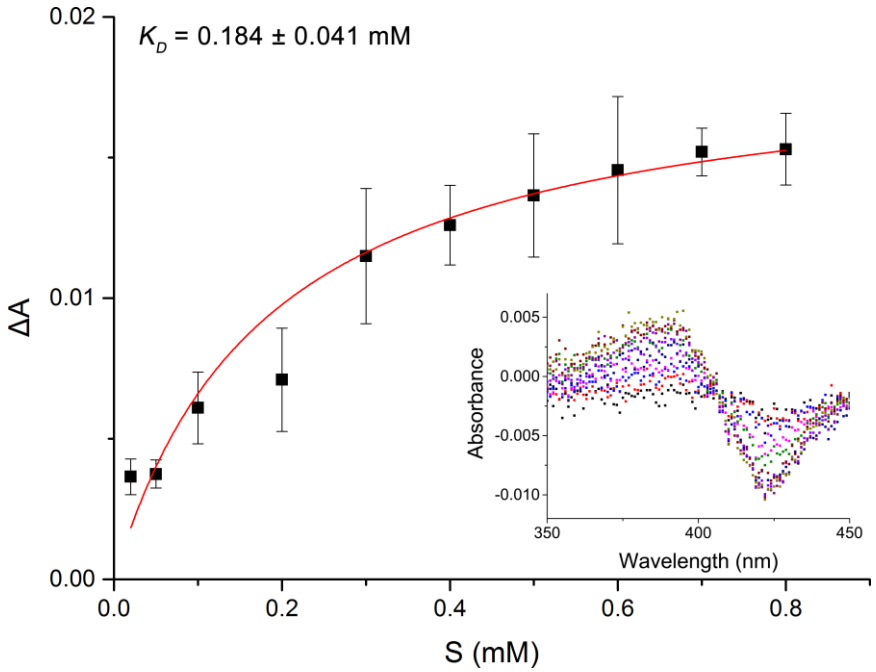

Fig. S12. The binding curve of 4-cresol to the W199A mutant.

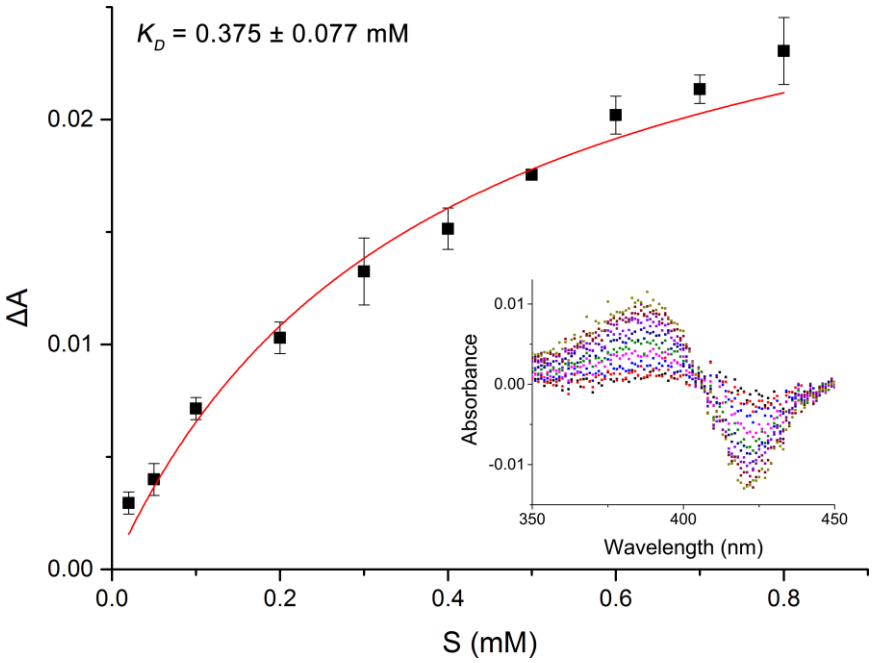

Fig. S13. The binding curve of 4-cresol to the I312A mutant.

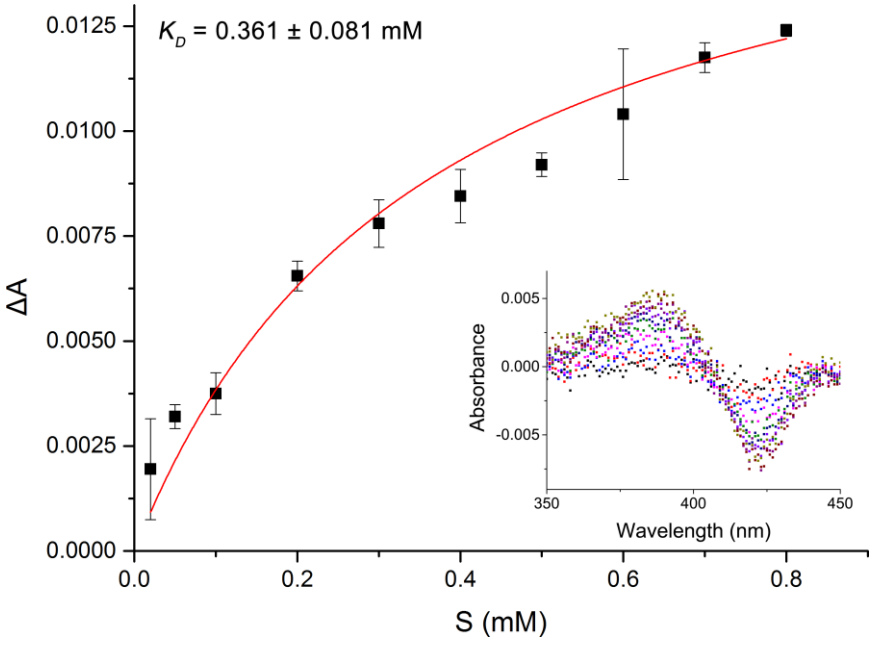

Fig. S14. The binding curve of 4-cresol to the F416A mutant.

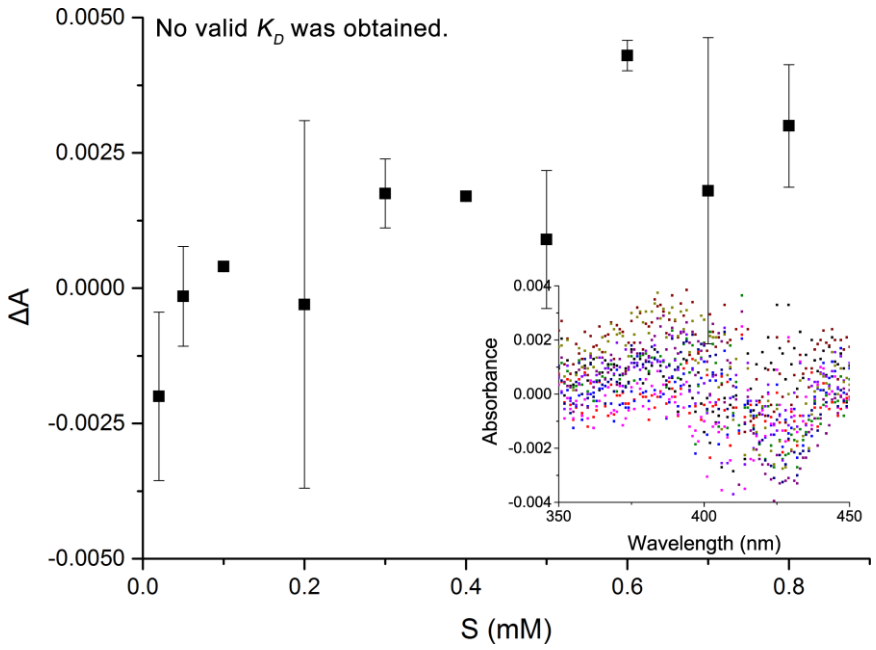

Fig. S15. The binding curve of 4-cresol to the F264A mutant.

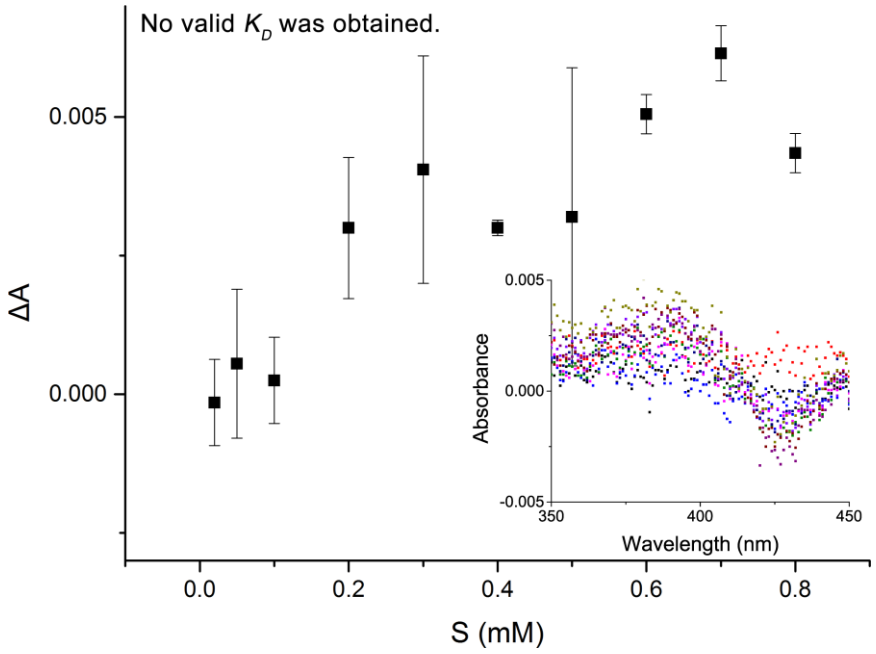

Fig. S16. The binding curve of 4-cresol to the W315A mutant.

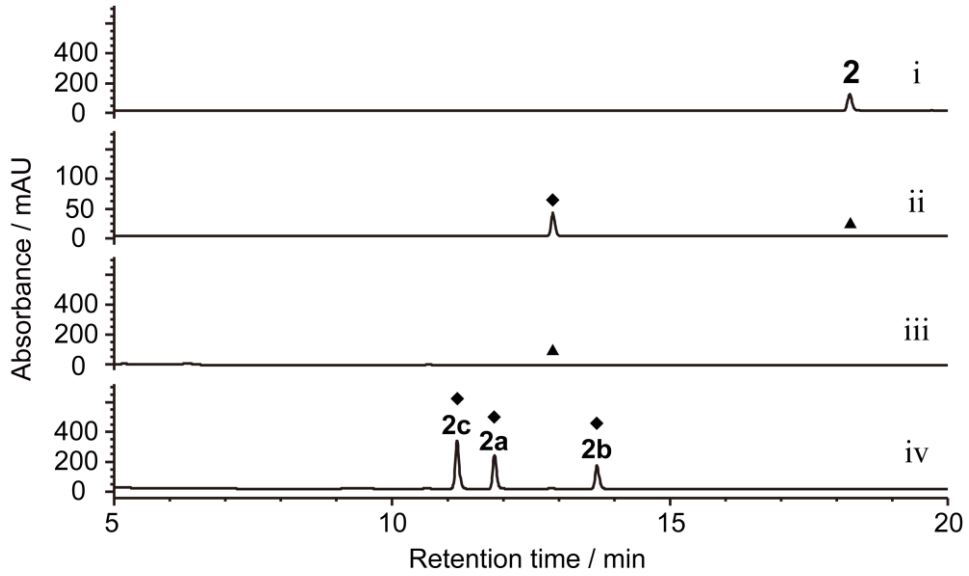

Fig. S17. Preliminary reactivity determination of CreHI, CreJEF and CreD towards 2 and its derivatives. Trace i, Negative control; trace ii, **2** + CreHI; trace iii, the post-CreHI reaction mixture + CreJEF; trace iv, the post-CreHI/CreJEF reaction mixture + CreD. ◆ indicates product generation compared to the upper trace. ▲ indicates significant substrate consumption compared to the upper trace.

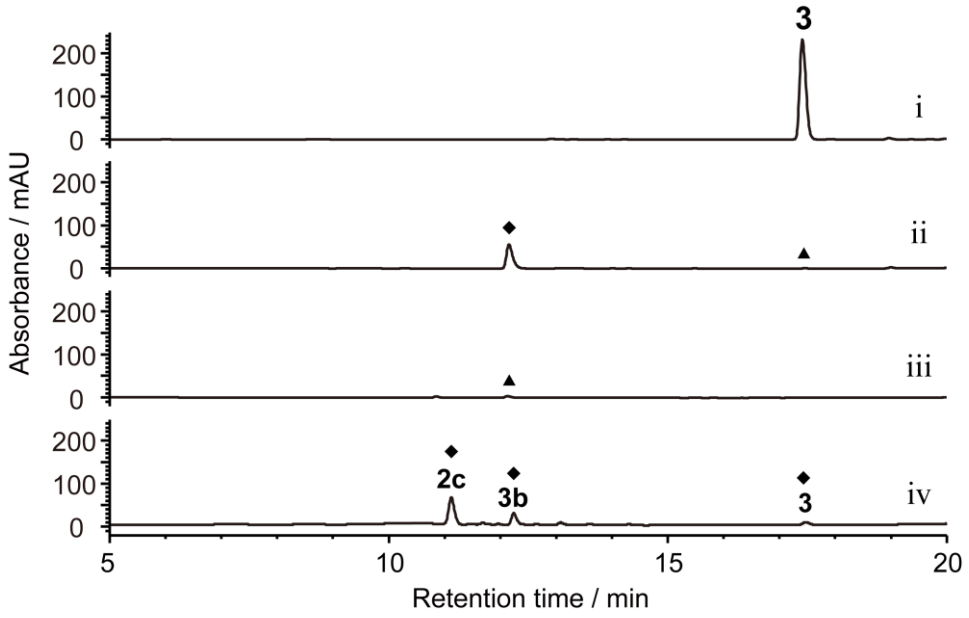

Fig. S18. Preliminary reactivity determination of CreHI, CreJEF and CreD towards 3 and its derivatives. Trace i, Negative control; trace ii, **3** + CreHI; trace iii, the post-CreHI reaction mixture + CreJEF; trace iv, the post-CreHI/CreJEF reaction mixture + CreD. ◆ indicates product generation compared to the upper trace. ▲ indicates significant substrate consumption compared to the upper trace.

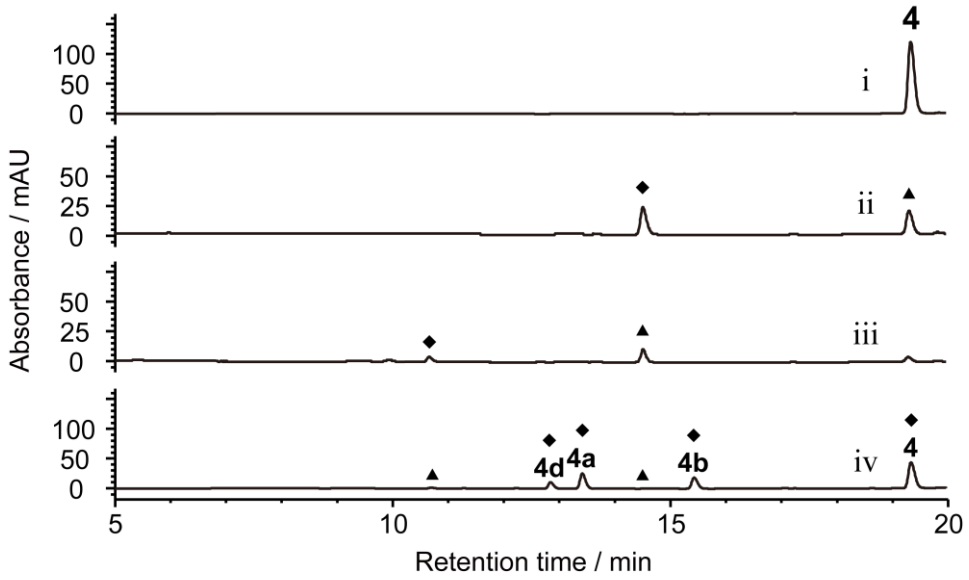

Fig. S19. Preliminary reactivity determination of CreHI, CreJEF and CreD towards 4 and its derivatives. Trace i, Negative control; trace ii, **4** + CreHI; trace iii, the post-CreHI reaction mixture + CreJEF; trace iv, the post-CreHI/CreJEF reaction mixture + CreD. ◆ indicates product generation compared to the upper trace. ▲ indicates significant substrate consumption compared to the upper trace.

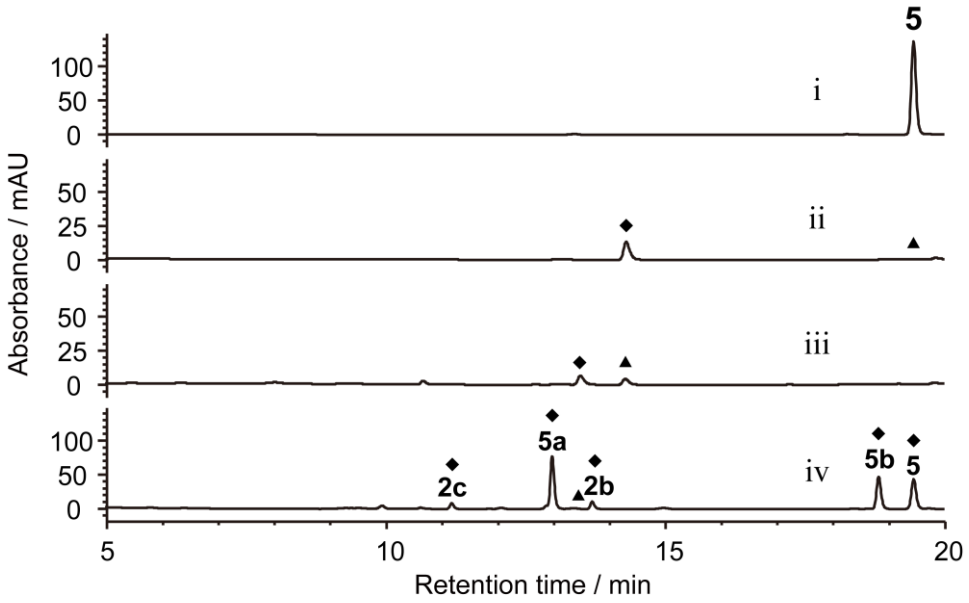

Fig. S20. Preliminary reactivity determination of CreHI, CreJEF and CreD towards 5 and its derivatives. Trace i, Negative control; trace ii, **5** + CreHI; trace iii, the post-CreHI reaction mixture + CreJEF; trace iv, the post-CreHI/CreJEF reaction mixture + CreD. ◆ indicates product generation compared to the upper trace. ▲ indicates significant substrate consumption compared to the upper trace.

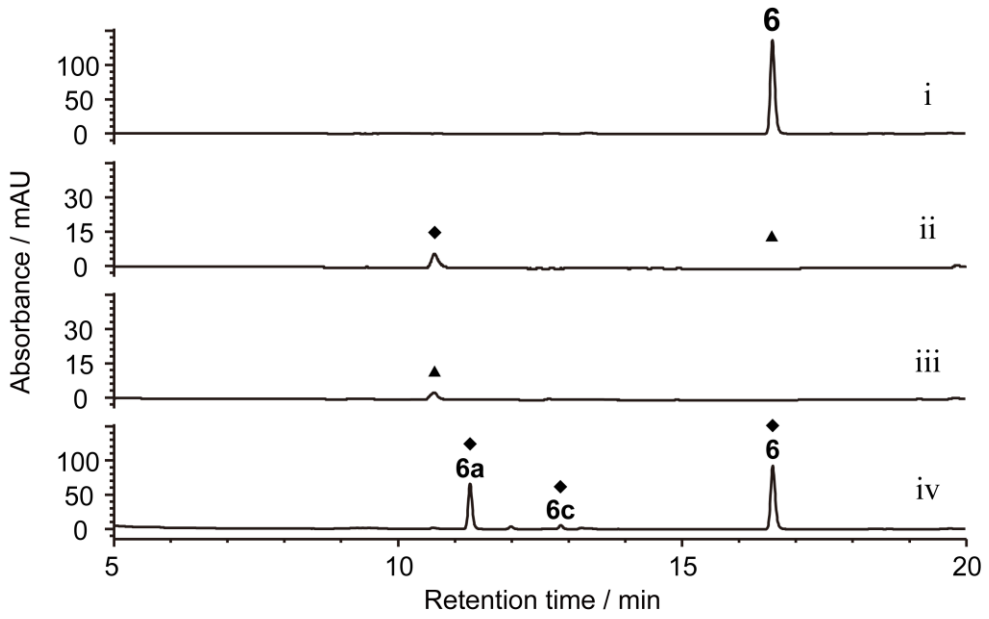

Fig. S21. Preliminary reactivity determination of CreHI, CreJEF and CreD towards 6 and its derivatives. Trace i, Negative control; trace ii, **6** + CreHI; trace iii, the post-CreHI reaction mixture + CreJEF; trace iv, the post-CreHI/CreJEF reaction mixture + CreD. ◆ indicates product generation compared to the upper trace. ▲ indicates significant substrate consumption compared to the upper trace.

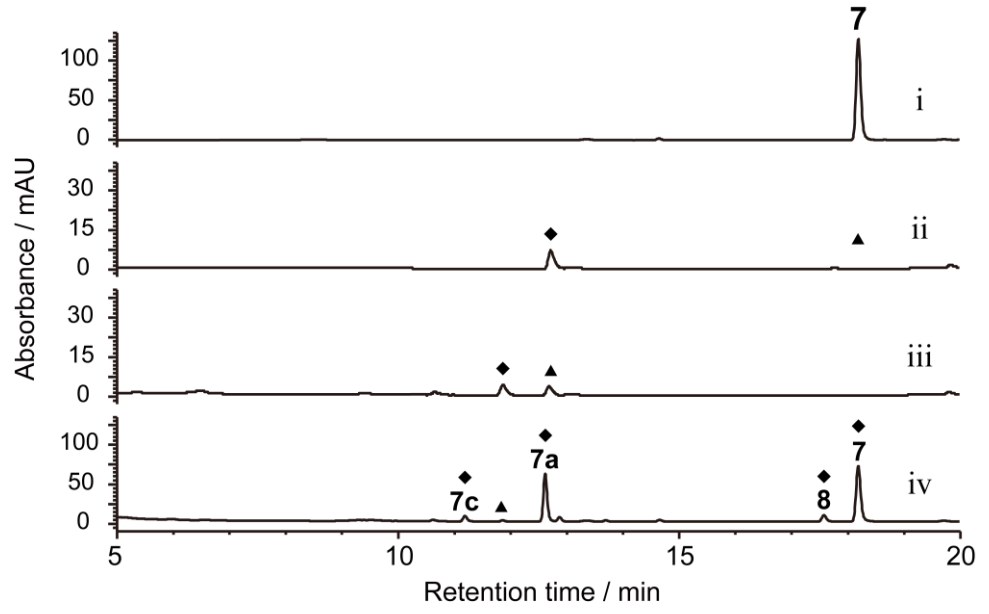

Fig. S22. Preliminary reactivity determination of CreHI, CreJEF and CreD towards 7 and its derivatives. Trace i, Negative control; trace ii, **7** + CreHI; trace iii, the post-CreHI reaction mixture + CreJEF; trace iv, the post-CreHI/CreJEF reaction mixture + CreD. ◆ indicates product generation compared to the upper trace. ▲ indicates significant substrate consumption compared to the upper trace.

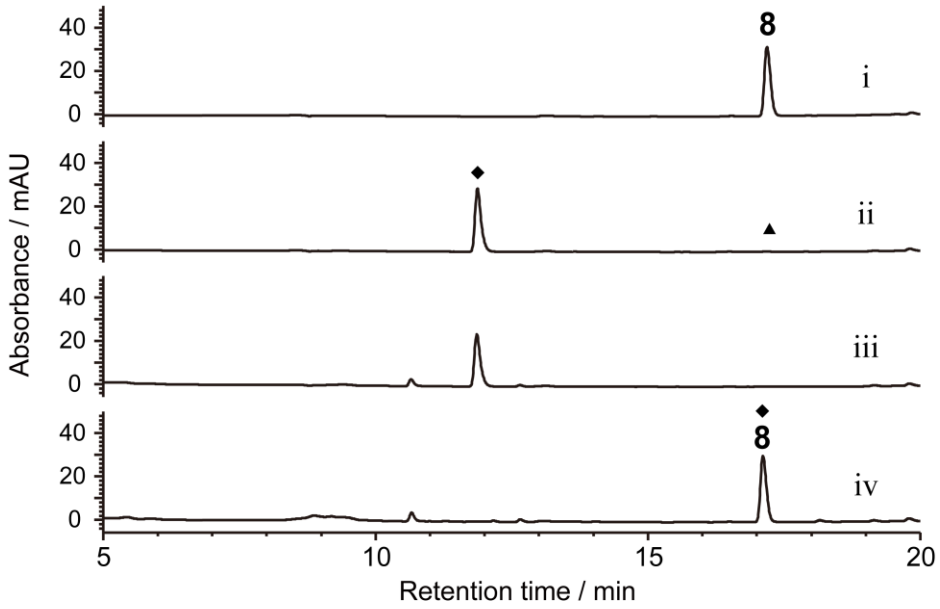

Fig. S23. Preliminary reactivity determination of CreHI, CreJEF and CreD towards 8 and its derivatives. Trace i, Negative control; trace ii, **8** + CreHI; trace iii, the post-CreHI reaction mixture + CreJEF; trace iv, the post-CreHI/CreJEF reaction mixture + CreD. ◆ indicates product generation compared to the upper trace. ▲ indicates significant substrate consumption compared to the upper trace.

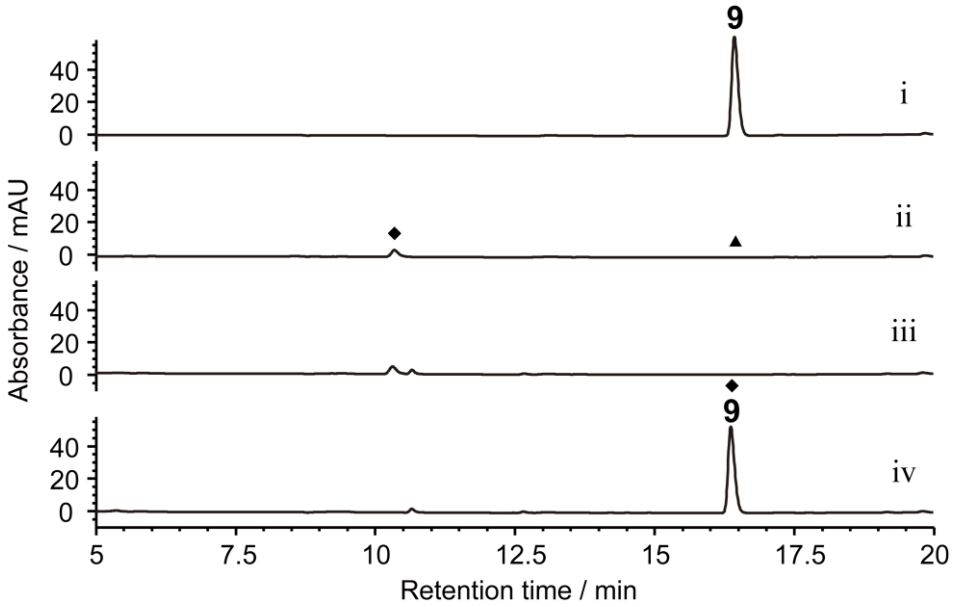

Fig. S24. Preliminary reactivity determination of CreHI, CreJEF and CreD towards 9 and its derivatives. Trace i, Negative control; trace ii, **9** + CreHI; trace iii, the post-CreHI reaction mixture + CreJEF; trace iv, the post-CreHI/CreJEF reaction mixture + CreD. ◆ indicates product generation compared to the upper trace. ▲ indicates significant substrate consumption compared to the upper trace.

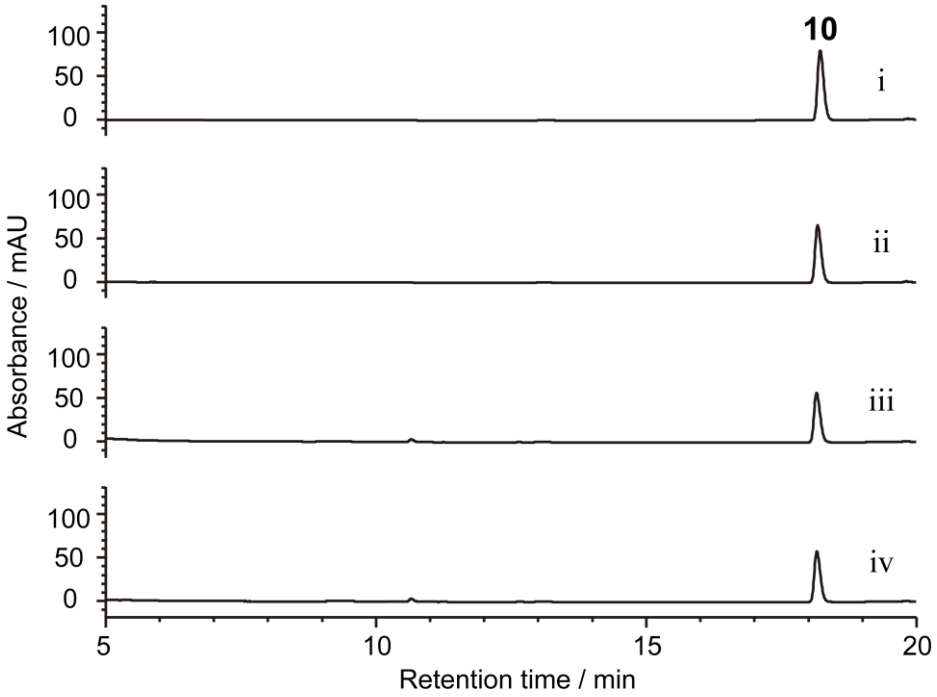

Fig. S25. Preliminary reactivity determination of CreHI, CreJEF and CreD towards 10 and its derivatives. Trace i, Negative control; trace ii, **10** + CreHI; trace iii, the post-CreHI reaction mixture + CreJEF; trace iv, the post-CreHI/CreJEF reaction mixture + CreD.

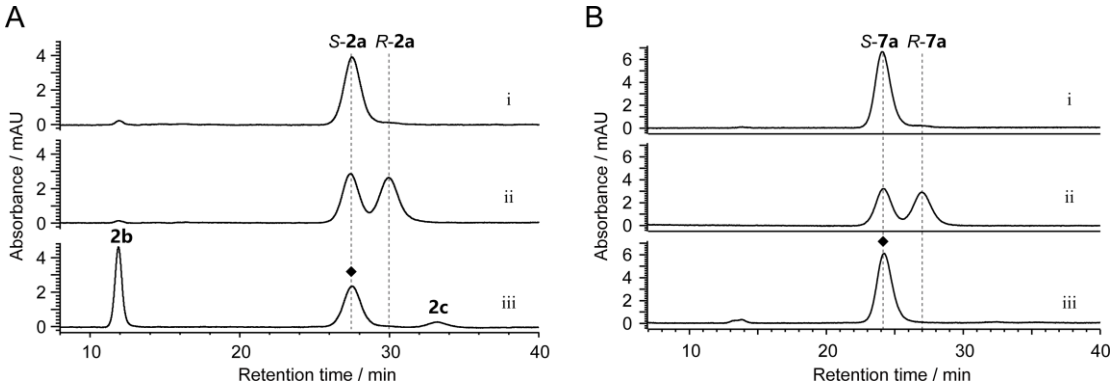

Fig. S26. Determination of the absolute configuration of 2a (*A*) and 7a (*B*) by chiral HPLC analysis. (*A*) Trace i, *S*-**2a** authentic standard; trace ii, racemic **2a** standard; trace iii, the reaction mixture of **2** sequentially reacted with CreHI/CreJEF and CreD. ◆ indicates only *S*-**2a** was produced. (*B*) Trace i, *S*-**7a** authentic standard; trace ii, racemic **7a** standard; trace iii, the reaction mixture of **7** sequentially reacted with CreHI/CreJEF and CreD. ◆ indicates only *S*-**7a** was produced.

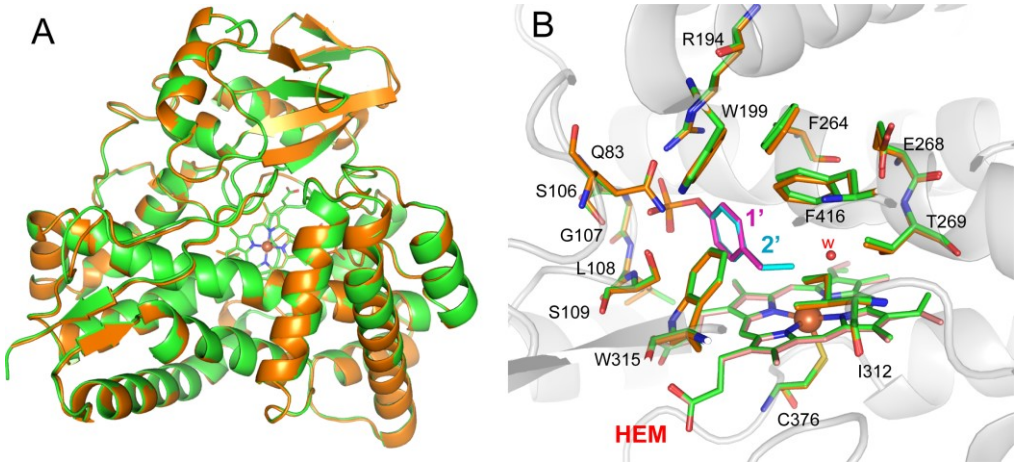

Fig. S27. Structural comparison of CreJ-1' (green, 5GWE) and CreJ-2' (orange, 5XJN). (*A*) Superimposition of CreJ-**1'** and CreJ-**2'**. (B) Conformational alignment of the active site residues. Substrate **1'** and **2'** are shown in purple and cyan, respectively. "w" represents the water molecule observed only in the CreJ-**1'** structure.

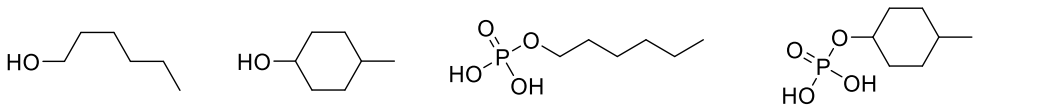

Fig. S28. Structures of non-aromatic 11, 12, 11' and 12'.

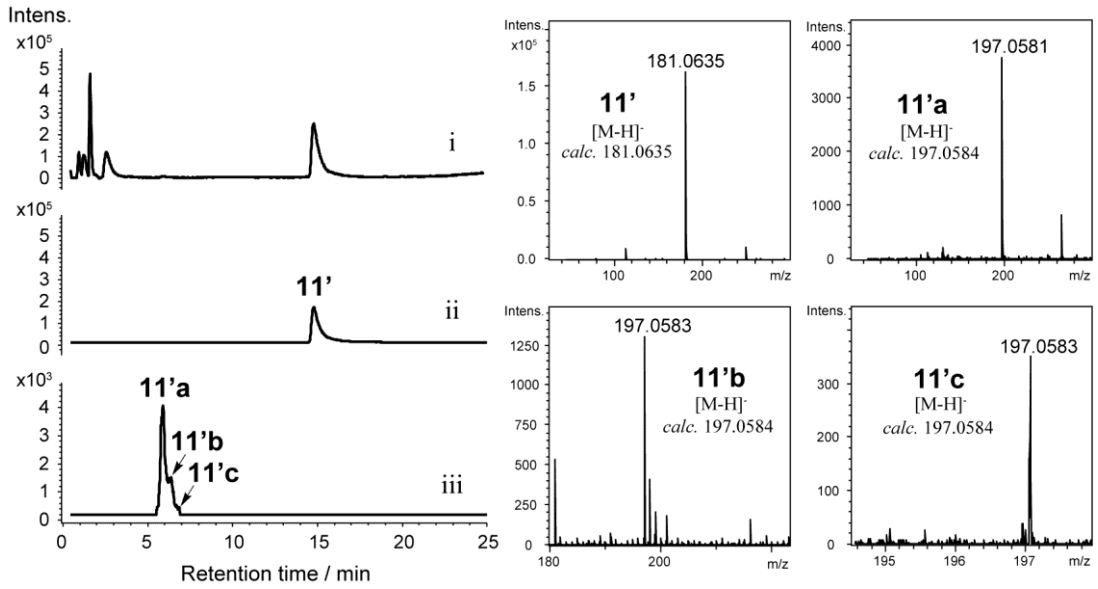

Fig. S29. LC-HRMS analysis of the CreJ reactivity towards 11'. Trace i, the total ion chromatography (TIC) of the CreJEF catalyzed reaction with **11'** as substrate; trace ii, the extract ion chromatography at m/z 181; trace iii, the extract ion chromatography at m/z 197. The right panel shows the high resolution mass spectra of **11'** and **11'a-c**.

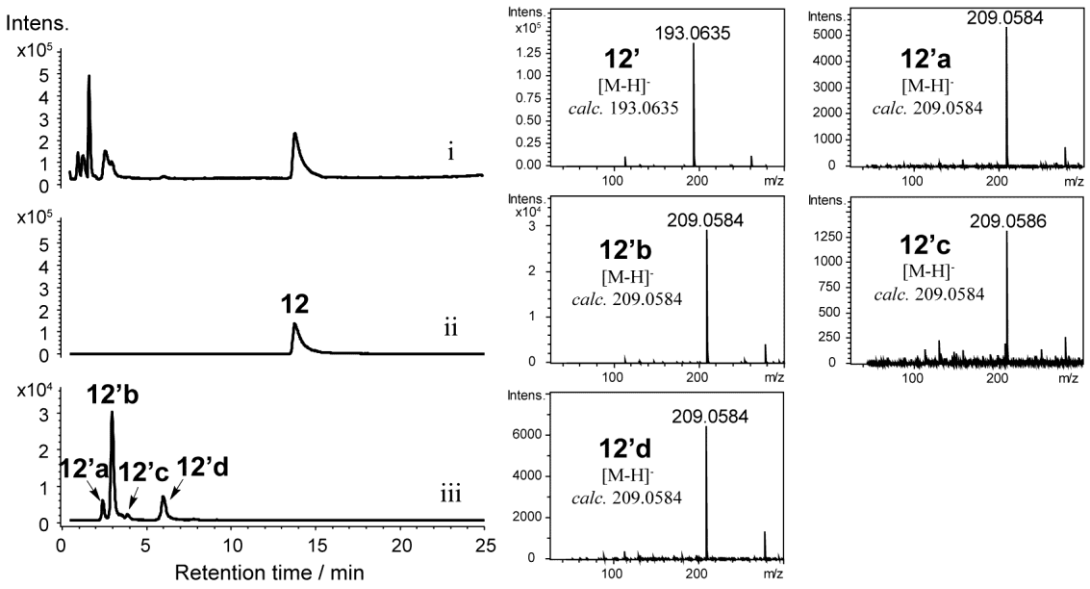

Fig. S30. LC-HRMS analysis of the CreJ reactivity towards 12'. Trace i, the total ion chromatography (TIC) of the CreJEF catalyzed reaction with **12'** as substrate; trace ii, the extract ion chromatography at m/z 193; trace iii, the extract ion chromatography at m/z 209. The right panel shows the high resolution mass spectra of **12'** and **12'a-d**.

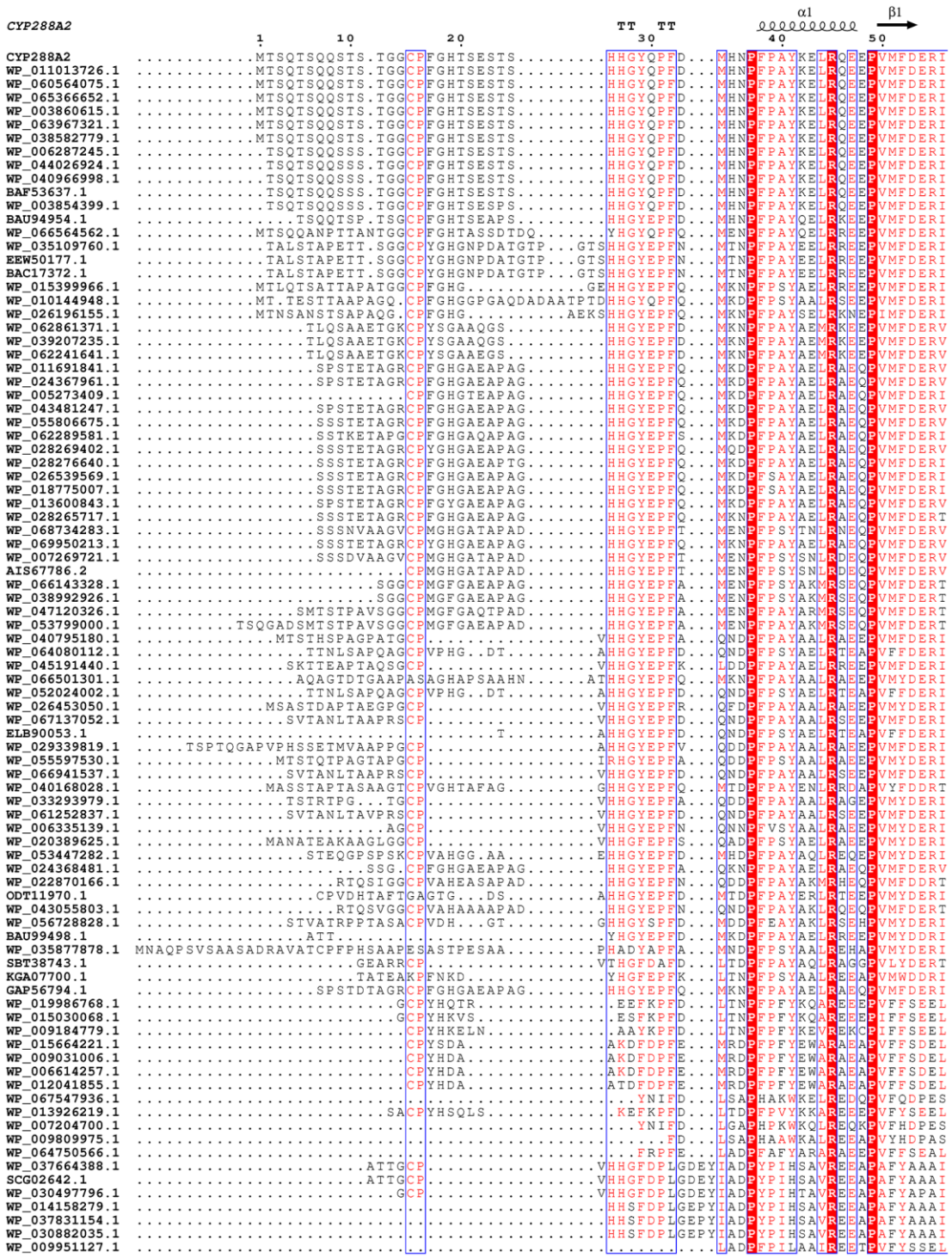
CYP288A2
α1
β1
TT TT
1
10
20
30
40
50
CYP288A2
WP_011013726.1
WP_060564075.1
WP_065366652.1
WP_003860615.1
WP_063967321.1
WP_038582779.1
WP_006287245.1
WP_044026924.1
WP_040966998.1
BAF53637.1
WP_003854399.1
BAU94954.1
WP_066564562.1
WP_035109760.1
EEW50177.1
BAC17372.1
WP_015399966.1
WP_010144948.1
WP_026196155.1
WP_062861371.1
WP_039207235.1
WP_062241641.1
WP_011691841.1
WP_024367961.1
WP_005273409.1
WP_043481247.1
WP_055806675.1
WP_062289581.1
WP_028269402.1
WP_028276640.1
WP_026539569.1
WP_018775007.1
WP_013600843.1
WP_028265717.1
WP_068734283.1
WP_069950213.1
WP_007269721.1
AIS67786.2
WP_066143328.1
WP_038992926.1
WP_047120326.1
WP_053799000.1
WP_040795180.1
WP_064080112.1
WP_045191440.1
WP_066501301.1
WP_052024002.1
WP_026453050.1
WP_067137052.1
ELB90053.1
WP_029339819.1
WP_055597530.1
WP_066941537.1
WP_040168028.1
WP_033293979.1
WP_061252837.1
WP_006335139.1
WP_020389625.1
WP_053447282.1
WP_024368481.1
WP_022870166.1
ODT11970.1
WP_043055803.1
WP_056728828.1
BAU99498.1
WP_035877878.1
SBT38743.1
KGA07700.1
GAP56794.1
WP_019986768.1
WP_015030068.1
WP_009184779.1
WP_015664221.1
WP_009031006.1
WP_006614257.1
WP_012041855.1
WP_067547936.1
WP_013926219.1
WP_007204700.1
WP_009809975.1
WP_064750566.1
WP_037664388.1
SCG02642.1
WP_030497796.1
WP_014158279.1
WP_037831154.1
WP_030882035.1
WP_009951127.1

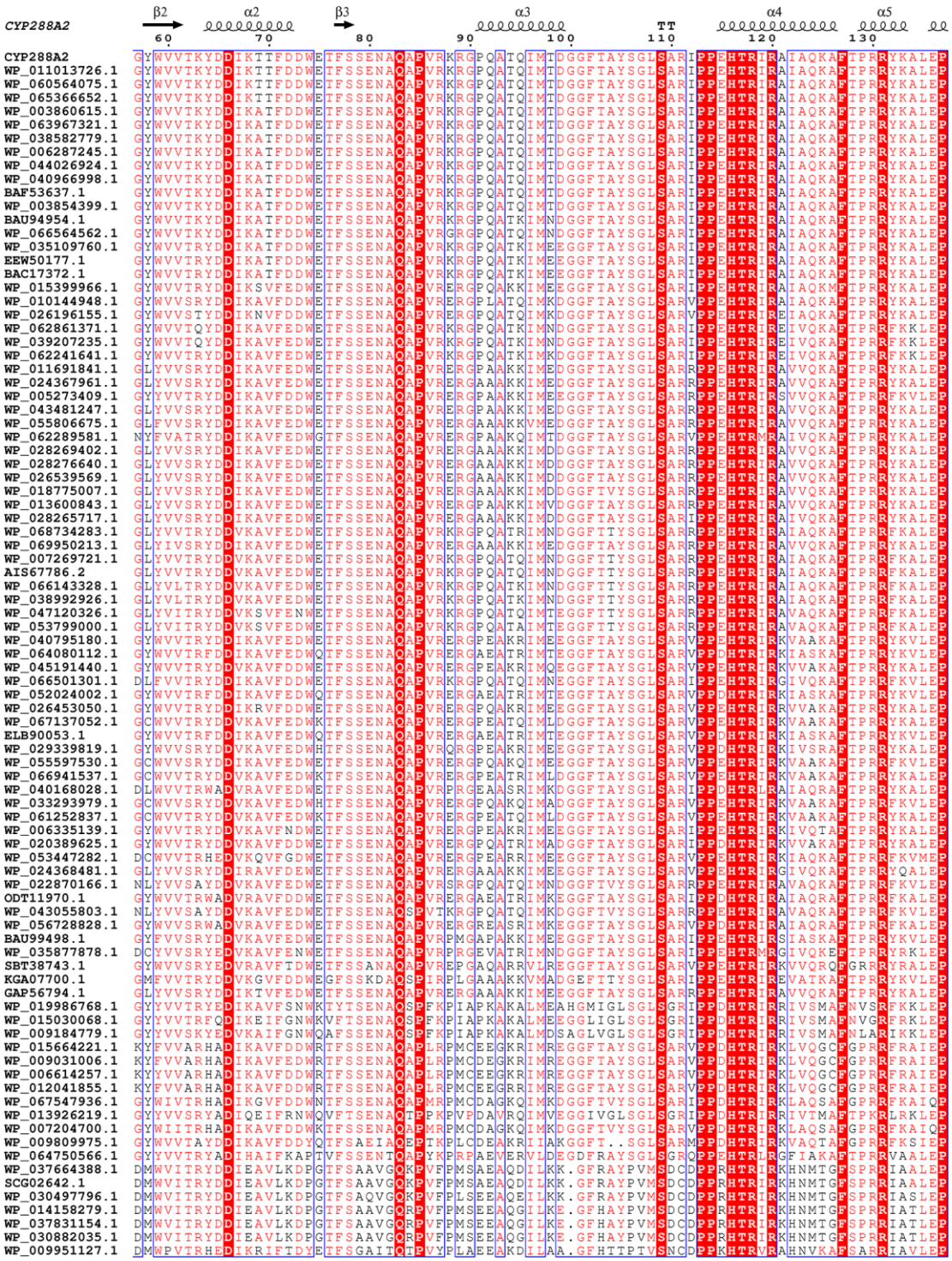
CYP288A2
β2
α2
β3
α3
TT
α4
α5
60
70
80
90
100
110
120
130
CYP288A2
WP_011013726.1
WP_060564075.1
WP_065366652.1
WP_003860615.1
WP_063967321.1
WP_038582779.1
WP_006287245.1
WP_044026924.1
WP_040966998.1
BAF53637.1
WP_003854399.1
BAU94954.1
WP_066564562.1
WP_035109760.1
EEW50177.1
BAC17372.1
WP_015399966.1
WP_010144948.1
WP_026196155.1
WP_062861371.1
WP_039207235.1
WP_062241641.1
WP_011691841.1
WP_024367961.1
WP_005273409.1
WP_043481247.1
WP_055806675.1
WP_062289581.1
WP_028269402.1
WP_028276640.1
WP_026539569.1
WP_018775007.1
WP_013600843.1
WP_028265717.1
WP_068734283.1
WP_069950213.1
WP_007269721.1
AIS67786.2
WP_066143328.1
WP_038992926.1
WP_047120326.1
WP_053799000.1
WP_040795180.1
WP_064080112.1
WP_045191440.1
WP_066501301.1
WP_052024002.1
WP_026453050.1
WP_067137052.1
ELB90053.1
WP_029339819.1
WP_055597530.1
WP_066941537.1
WP_040168028.1
WP_033293979.1
WP_061252837.1
WP_006335139.1
WP_020389625.1
WP_053447282.1
WP_024368481.1
WP_022870166.1
ODT11970.1
WP_043055803.1
WP_056728828.1
BAU99498.1
WP_035877878.1
SBT38743.1
KGA07700.1
GAP56794.1
WP_019986768.1
WP_015030068.1
WP_009184779.1
WP_015664221.1
WP_009031006.1
WP_006614257.1
WP_012041855.1
WP_067547936.1
WP_013926219.1
WP_007204700.1
WP_009809975.1
WP_064750566.1
WP_037664388.1
SCG02642.1
WP_030497796.1
WP_014158279.1
WP_037831154.1
WP_030882035.1
WP_009951127.1


α6
TT
β4
π1
α7
η1
α8
CYP288A2
140
150
160
170
180
190
200
210
CYP288A2
WP_011013726.1
WP_060564075.1
WP_065366652.1
WP_003860615.1
WP_063967321.1
WP_038582779.1
WP_006287245.1
WP_044026924.1
WP_040966998.1
BAF53637.1
WP_003854399.1
BAU94954.1
WP_066564562.1
WP_035109760.1
EEW50177.1
BAC17372.1
WP_015399966.1
WP_010144948.1
WP_026196155.1
WP_062861371.1
WP_039207235.1
WP_062241641.1
WP_011691841.1
WP_024367961.1
WP_005273409.1
WP_043481247.1
WP_055806675.1
WP_062289581.1
WP_028269402.1
WP_028276640.1
WP_026539569.1
WP_018775007.1
WP_013600843.1
WP_028265717.1
WP_068734283.1
WP_069950213.1
WP_007269721.1
AIS67786.2
WP_066143328.1
WP_038992926.1
WP_047120326.1
WP_053799000.1
WP_040795180.1
WP_064080112.1
WP_045191440.1
WP_066501301.1
WP_052024002.1
WP_026453050.1
WP_067137052.1
ELB90053.1
WP_029339819.1
WP_055597530.1
WP_066941537.1
WP_040168028.1
WP_033293979.1
WP_061252837.1
WP_006335139.1
WP_020389625.1
WP_053447282.1
WP_024368481.1
WP_022870166.1
ODT11970.1
WP_043055803.1
WP_056728828.1
BAU99498.1
WP_035877878.1
SBT38743.1
KGA07700.1
GAP56794.1
WP_019986768.1
WP_015030068.1
WP_009184779.1
WP_015664221.1
WP_009031006.1
WP_006614257.1
WP_012041855.1
WP_067547936.1
WP_013926219.1
WP_007204700.1
WP_009809975.1
WP_064750566.1
WP_037664388.1
SCG02642.1
WP_030497796.1
WP_014158279.1
WP_037831154.1
WP_030882035.1
WP_009951127.1


α9
α10
α11
CYP288A2
220
230
240
250
260
270
CYP288A2
WP_011013726.1
WP_060564075.1
WP_065366652.1
WP_003860615.1
WP_063967321.1
WP_038582779.1
WP_006287245.1
WP_044026924.1
WP_040966998.1
BAF53637.1
WP_003854399.1
BAU94954.1
WP_066564562.1
WP_035109760.1
EEW50177.1
BAC17372.1
WP_015399966.1
WP_010144948.1
WP_026196155.1
WP_062861371.1
WP_039207235.1
WP_062241641.1
WP_011691841.1
WP_024367961.1
WP_005273409.1
WP_043481247.1
WP_055806675.1
WP_062289581.1
WP_028269402.1
WP_028276640.1
WP_026539569.1
WP_018775007.1
WP_013600843.1
WP_028265717.1
WP_068734283.1
WP_069950213.1
WP_007269721.1
AIS67786.2
WP_066143328.1
WP_038992926.1
WP_047120326.1
WP_053799000.1
WP_040795180.1
WP_064080112.1
WP_045191440.1
WP_066501301.1
WP_052024002.1
WP_026453050.1
WP_067137052.1
ELB90053.1
WP_029339819.1
WP_055597530.1
WP_066941537.1
WP_040168028.1
WP_033293979.1
WP_061252837.1
WP_006335139.1
WP_020389625.1
WP_053447282.1
WP_024368481.1
WP_022870166.1
ODT11970.1
WP_043055803.1
WP_056728828.1
BAU99498.1
WP_035877878.1
SBT38743.1
KGA07700.1
GAP56794.1
WP_019986768.1
WP_015030068.1
WP_009184779.1
WP_015664221.1
WP_009031006.1
WP_006614257.1
WP_012041855.1
WP_067547936.1
WP_013926219.1
WP_007204700.1
WP_009809975.1
WP_064750566.1
WP_037664388.1
SCG02642.1
WP_030497796.1
WP_014158279.1
WP_037831154.1
WP_030882035.1
WP_009951127.1


α12
α13
η2
α14
β5
β6
β7
β8
α15
CYP288A2
280
290
300
310
320
330
340
350
CYP288A2
WP_011013726.1
WP_060564075.1
WP_065366652.1
WP_003860615.1
WP_063967321.1
WP_038582779.1
WP_006287245.1
WP_044026924.1
WP_040966998.1
BAF53637.1
WP_003854399.1
BAU94954.1
WP_066564562.1
WP_035109760.1
EEW50177.1
BAC17372.1
WP_015399966.1
WP_010144948.1
WP_026196155.1
WP_062861371.1
WP_039207235.1
WP_062241641.1
WP_011691841.1
WP_024367961.1
WP_005273409.1
WP_043481247.1
WP_055806675.1
WP_062289581.1
WP_028269402.1
WP_028276640.1
WP_026539569.1
WP_018775007.1
WP_013600843.1
WP_028265717.1
WP_068734283.1
WP_069950213.1
WP_007269721.1
AIS67786.2
WP_066143328.1
WP_038992926.1
WP_047120326.1
WP_053799000.1
WP_040795180.1
WP_064080112.1
WP_045191440.1
WP_066501301.1
WP_052024002.1
WP_026453050.1
WP_067137052.1
ELB90053.1
WP_029339819.1
WP_055597530.1
WP_066941537.1
WP_040168028.1
WP_033293979.1
WP_061252837.1
WP_006335139.1
WP_020389625.1
WP_053447282.1
WP_024368481.1
WP_022870166.1
ODT11970.1
WP_043055803.1
WP_056728828.1
BAU99498.1
WP_035877878.1
SBT38743.1
KGA07700.1
GAP56794.1
WP_019986768.1
WP_015030068.1
WP_009184779.1
WP_015664221.1
WP_009031006.1
WP_006614257.1
WP_012041855.1
WP_067547936.1
WP_013926219.1
WP_007204700.1
WP_009809975.1
WP_064750566.1
WP_037664388.1
SCG02642.1
WP_030497796.1
WP_014158279.1
WP_037831154.1
WP_030882035.1
WP_009951127.1

Fig. S31. Protein sequence alignment of CreJ homologues from diverse genera of microorganisms. Conserved residues are highlighted in white display with red background.

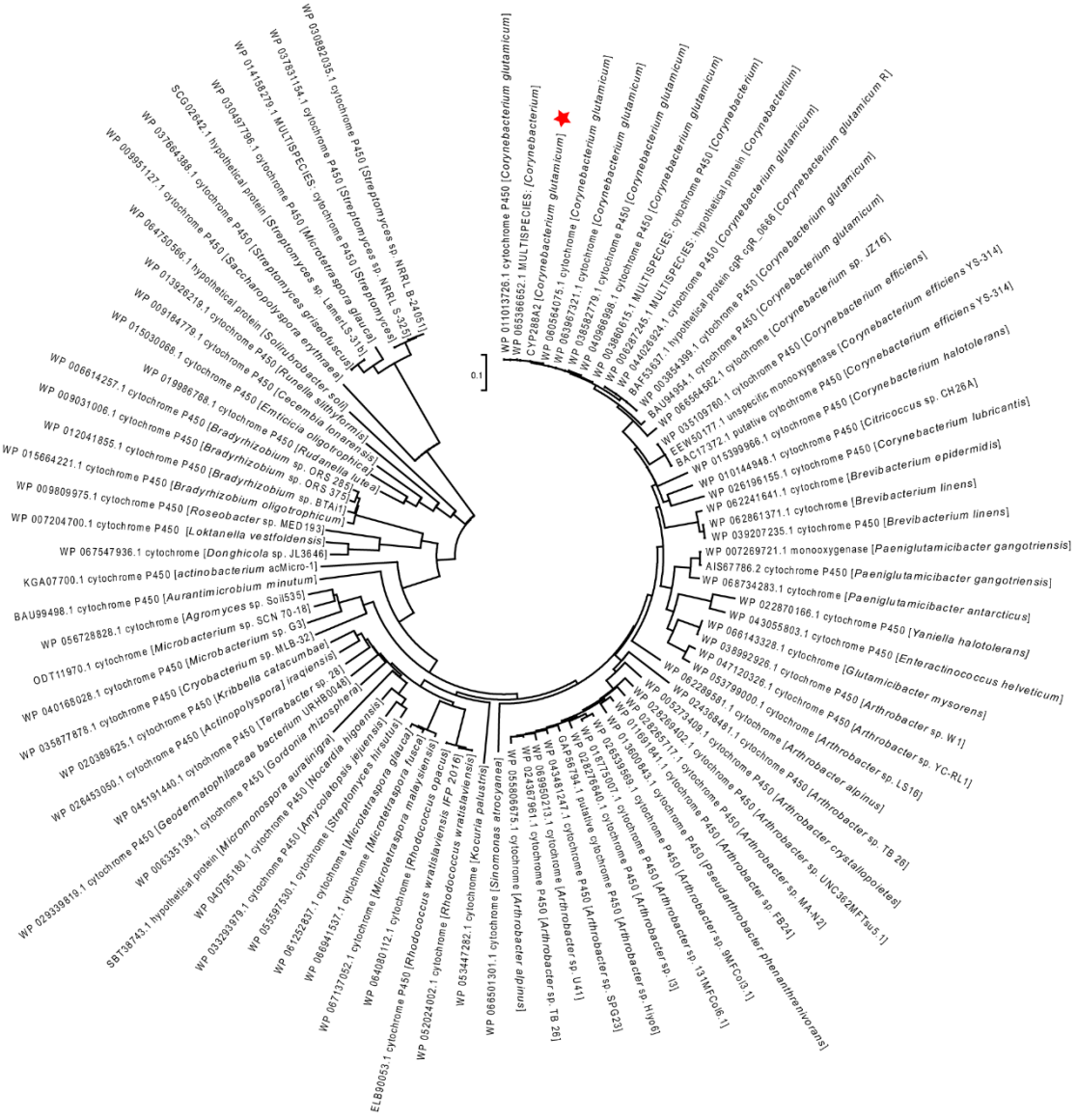

Fig. S32. Phylogenetic tree of CreJ homologues with > 40% protein sequence identity. CreJ (*i.e.* CYP288A2) is highlighted with the symbol of star.

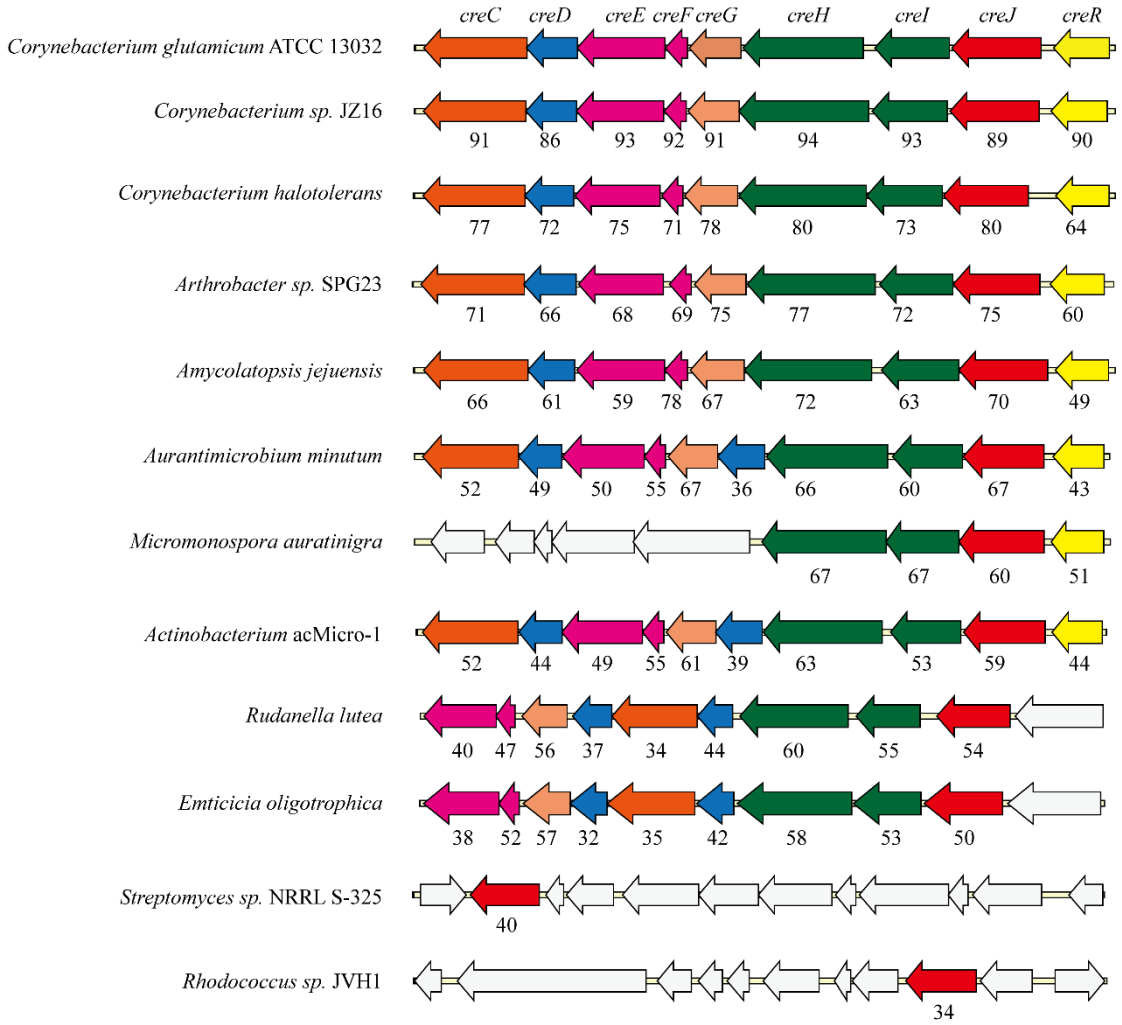

Fig. S33. Representations of *cre*-like gene clusters from diverse microorganisms. Arrows in a same color represent the homologous genes. Genes without colors have no homology to any *cre* genes. The number below the arrow indicates the percentage of protein sequence identity between the specific gene with its homologous gene in the *cre* cluster of *C. glutamicum* ATCC13032.

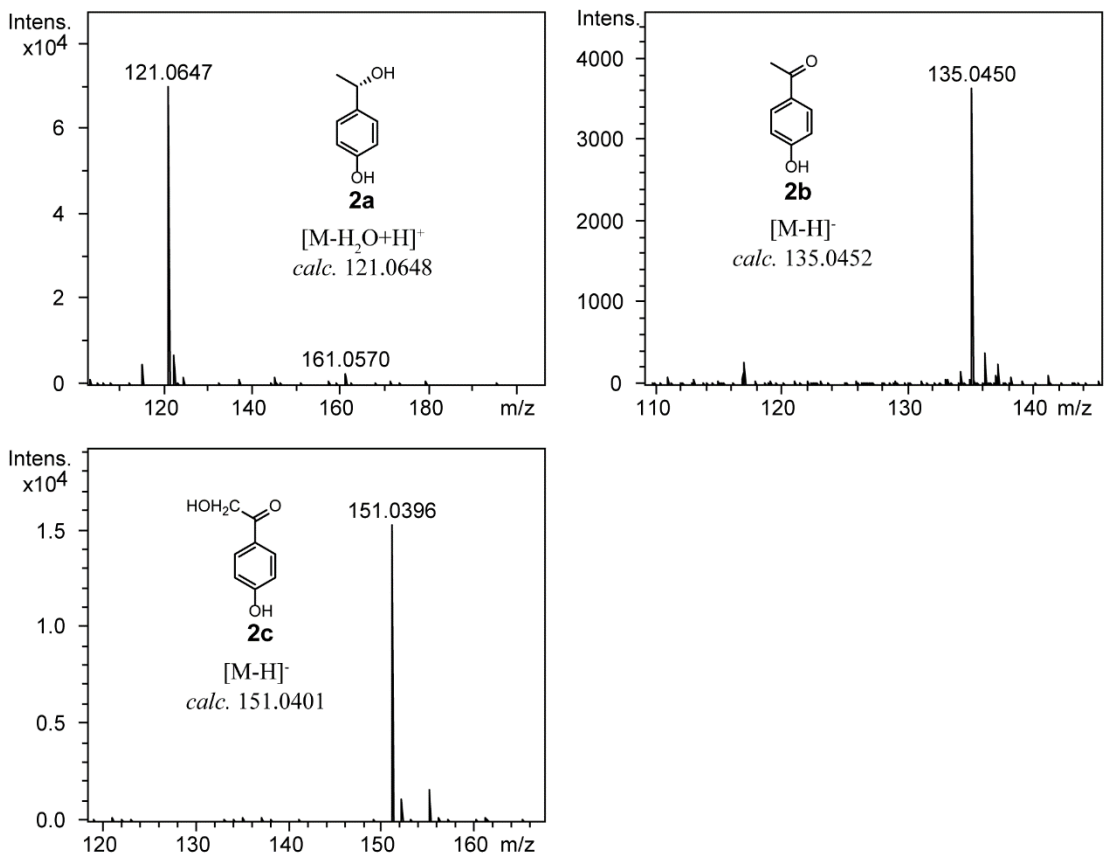

Fig. S34. HRMS spectra of oxidative products from 2.

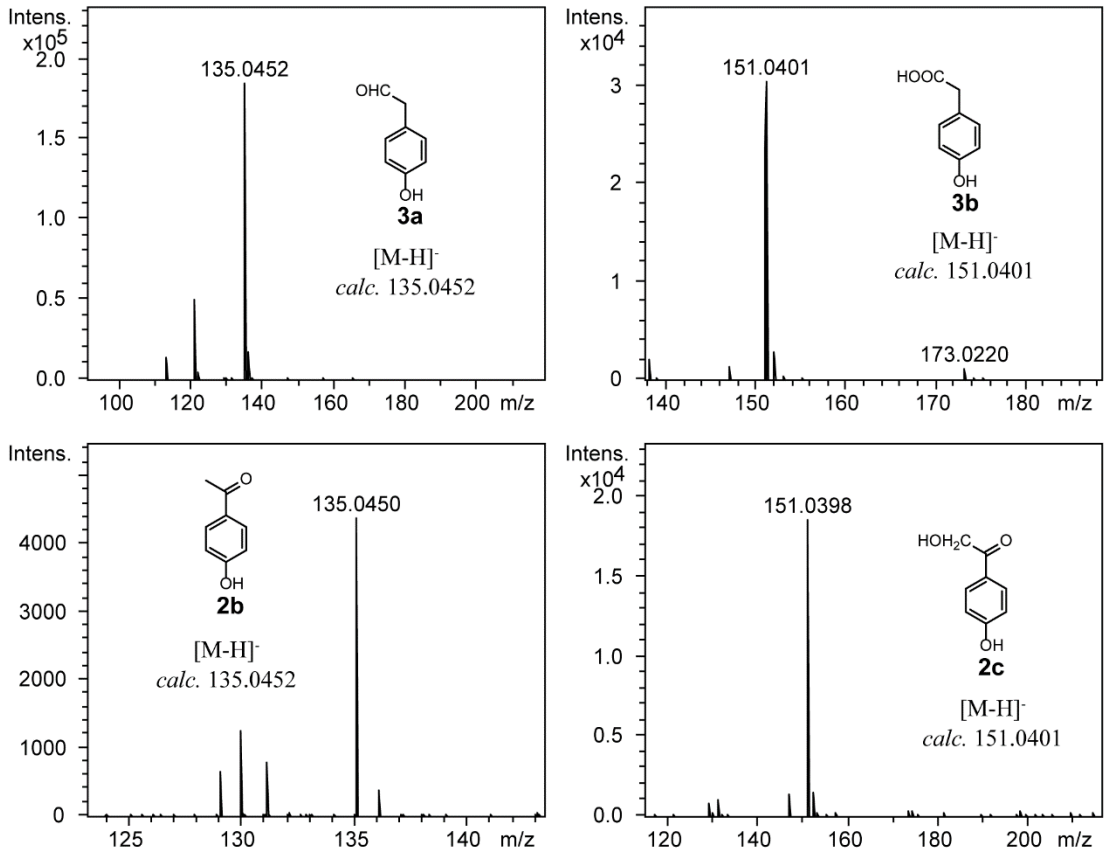

Fig. S35. HRMS spectra of oxidative products from 3.

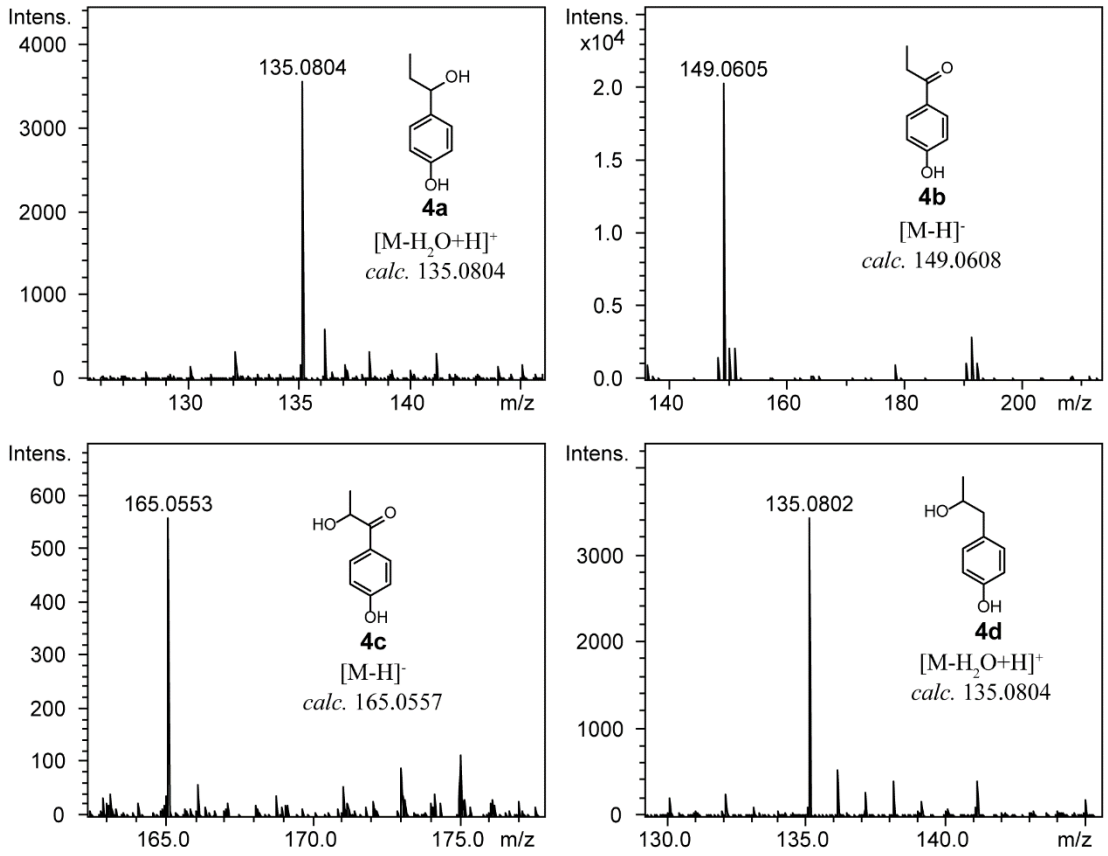

Fig. S36. HRMS spectra of oxidative products from 4.

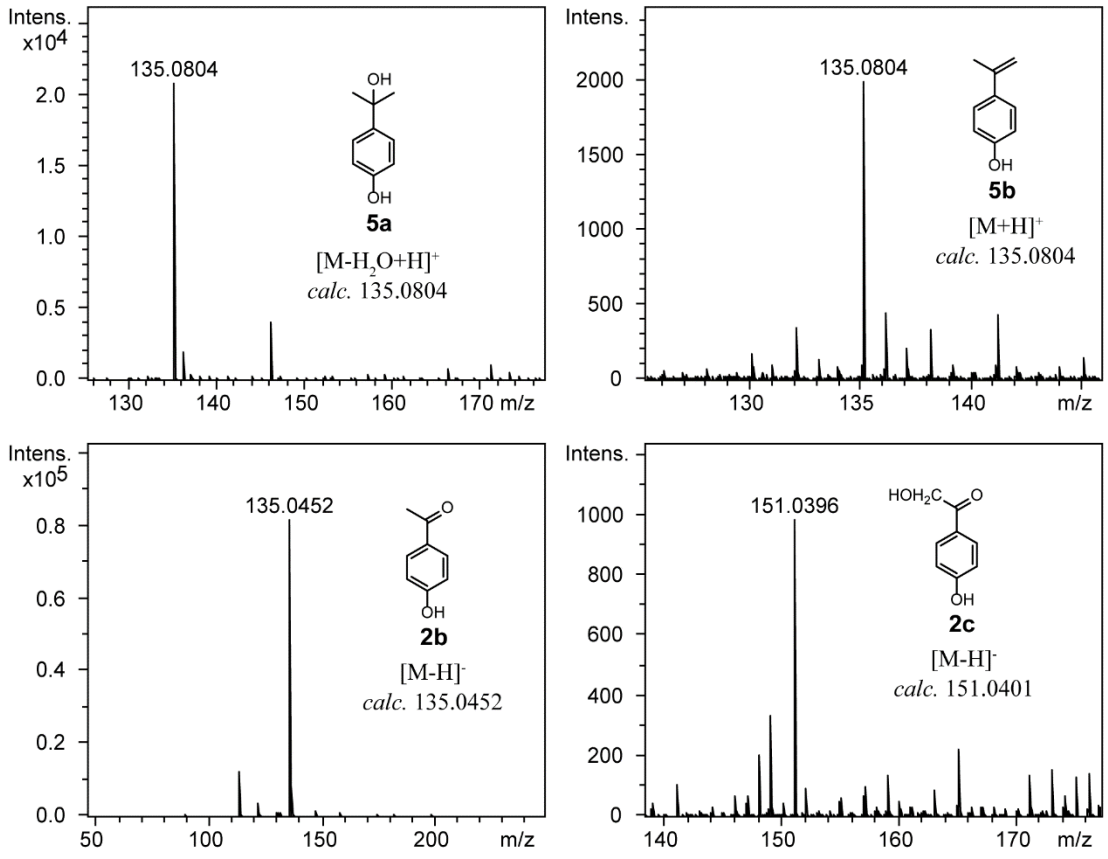

Fig. S37. HRMS spectra of oxidative products from 5.

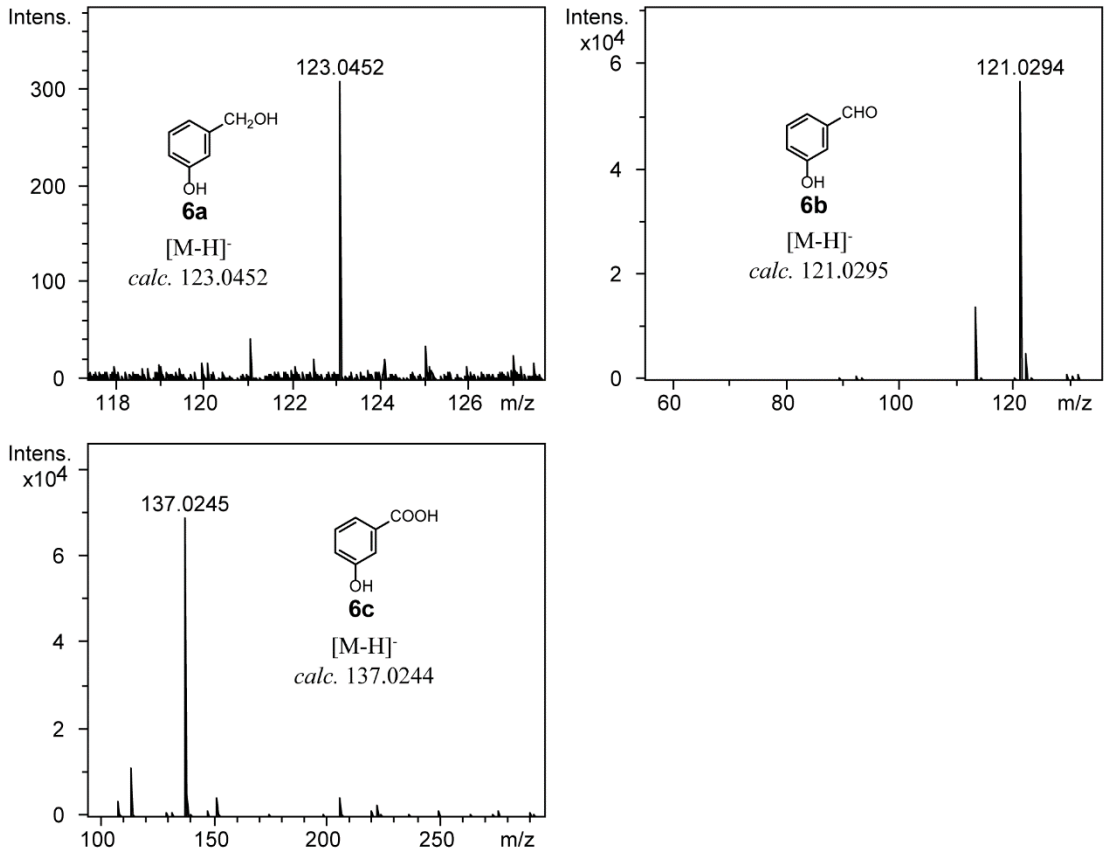

Fig. S38. HRMS spectra of oxidative products from 6.

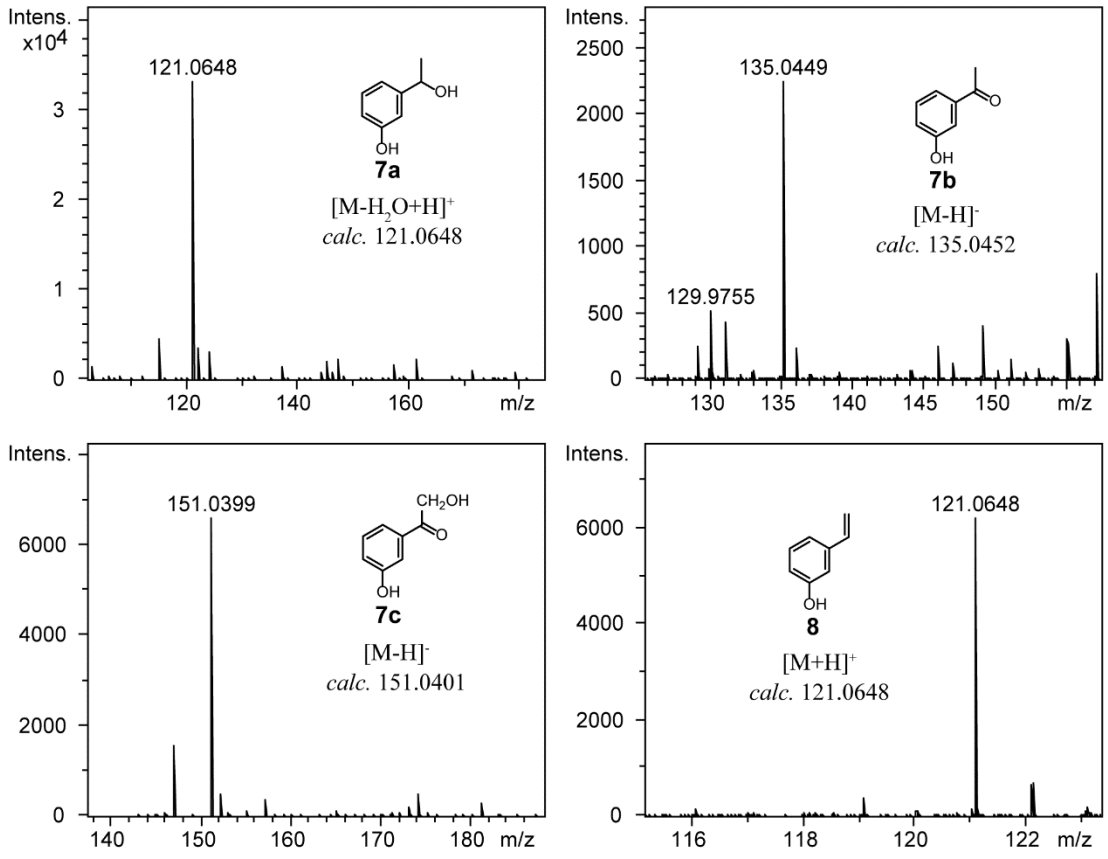

Fig. S39. HRMS spectra of oxidative products from 7.

Fig. S40. ^{1}H NMR spectrum of 2c in CD_3CN.

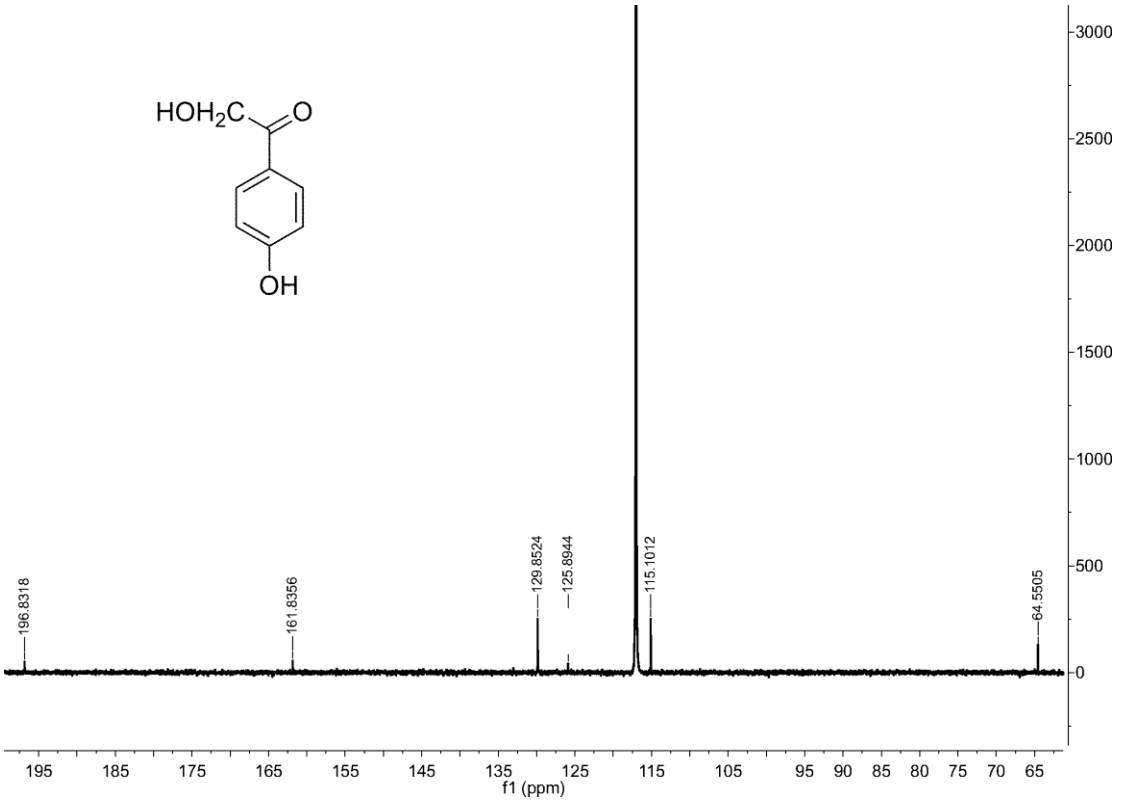

Fig. S41. ^{13}C NMR spectrum of 2c in CD_3CN.

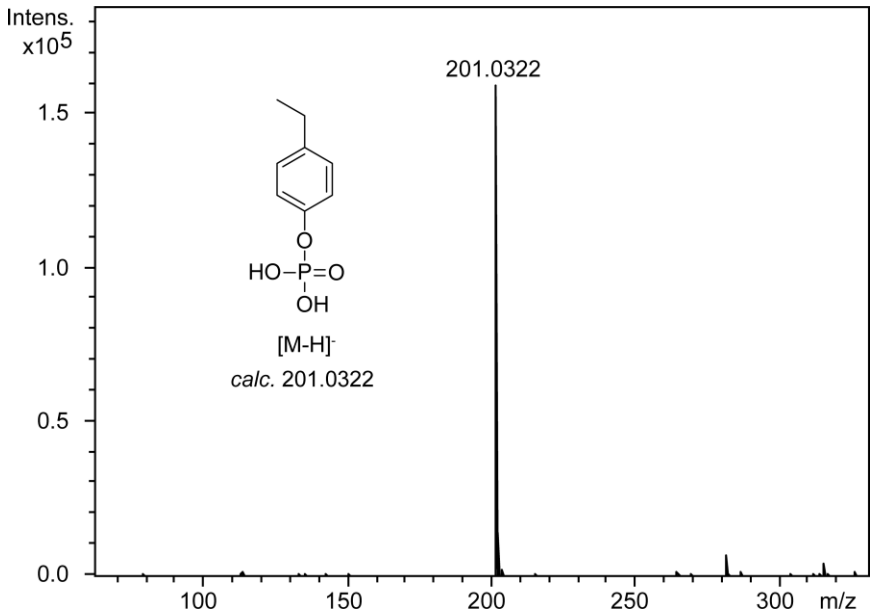

Fig. S42. HRMS of 2'.

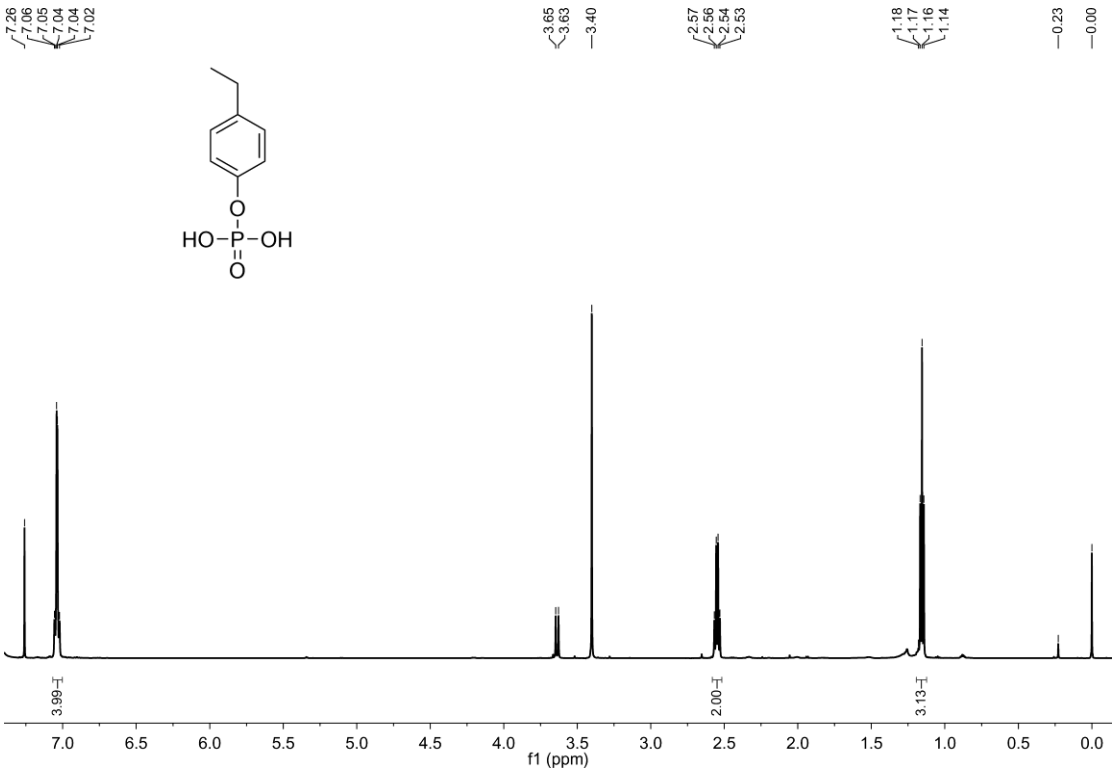

Fig. S43. ^{1}H NMR spectrum of 2' in CD_3CN.

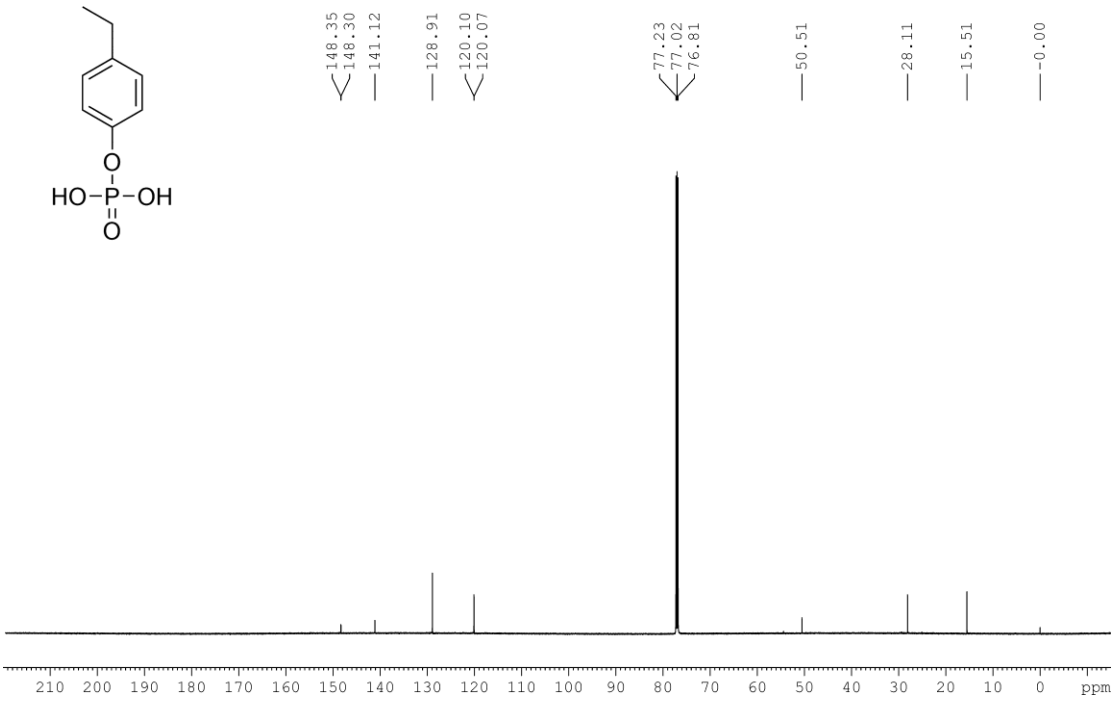

Fig. S44. ^{13}C NMR spectrum of 2' in CD_3CN.

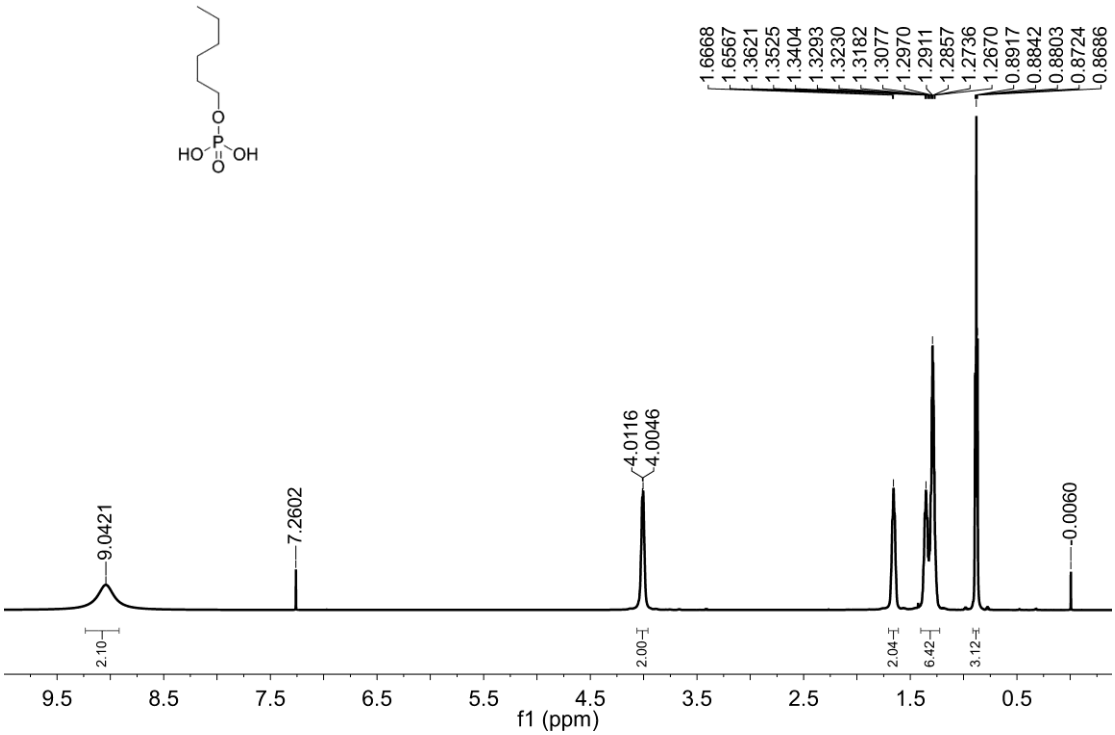

Fig. S45. ^{1}H NMR spectrum of 11' in $CDCl_3$.

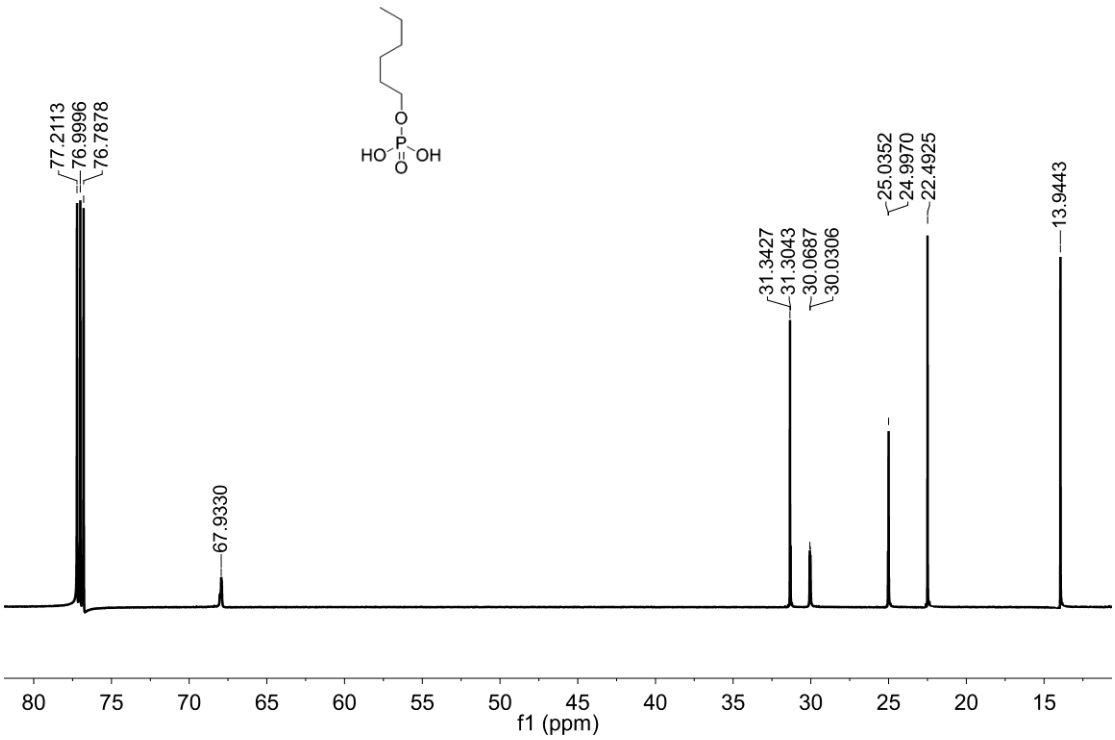

Fig. S46. ^{13}C NMR spectrum of 11' in $CDCl_3$.

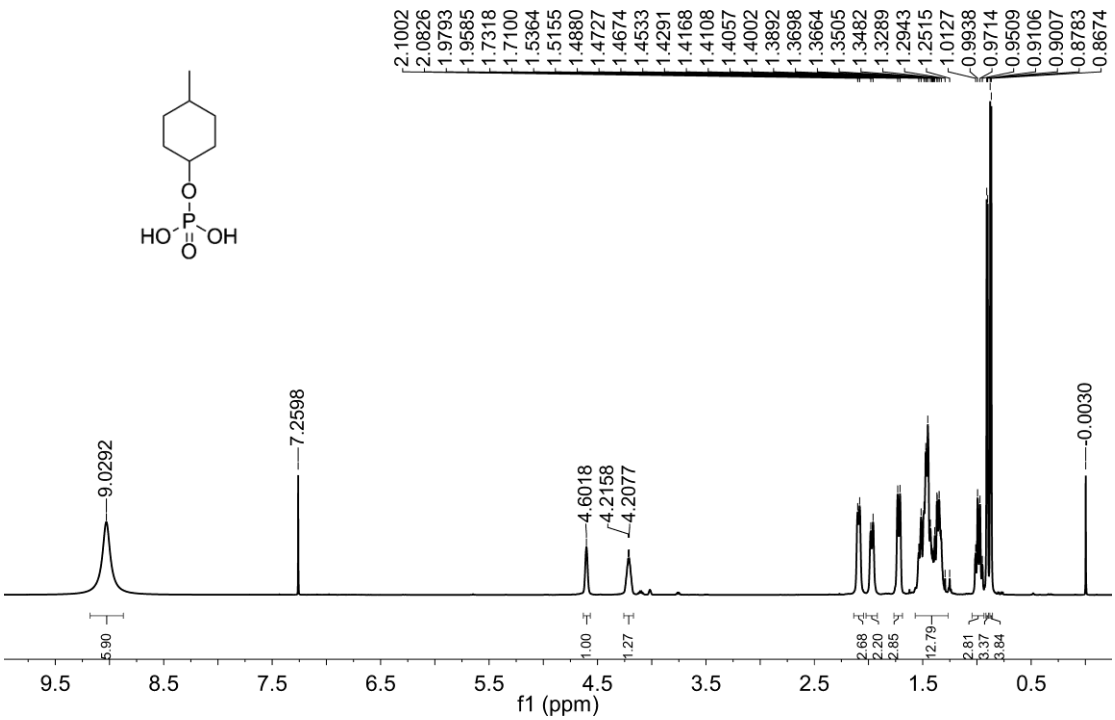

Fig. S47. ^{1}H NMR spectrum of 12' in $CDCl_3$.

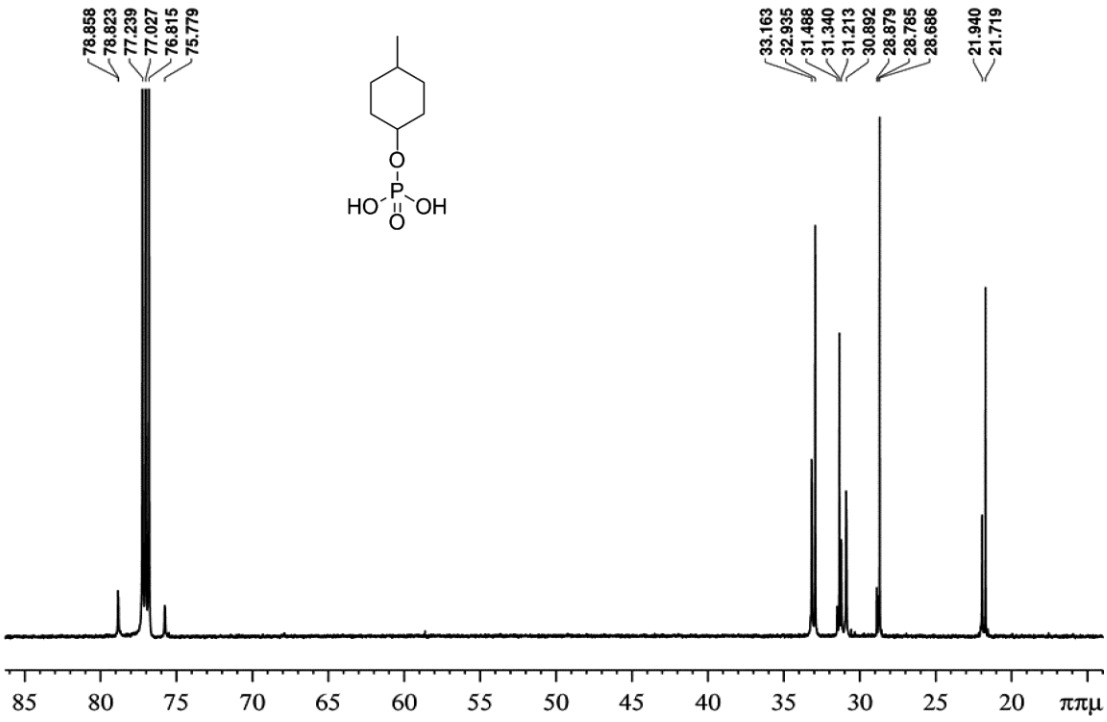

Fig. S48. ^{13}C NMR spectrum of 12' in $CDCl_3$.

References

1. Anzai Y*, et al.* (2008) Functional Analysis of MycCI and MycG, Cytochrome P450 Enzymes Involved in Biosynthesis of Mycinamicin Macrolide Antibiotics. *Chem Biol* 15(9):950-959.
2. Green MR & Sambrook J (2012) *Molecular Cloning: A Laboratory Manual (Fourth Edition)* (Cold Spring Harbor Laboratory Press, Cold Spring Harbor, New York).
3. Liu Y*, et al.* (2014) Hydrogen peroxide-independent production of alpha-alkenes by OleTJE P450 fatty acid decarboxylase. *Biotechnol Biofuels* 7(1):28.
4. Bradford MM (1976) A rapid and sensitive method for the quantitation of microgram quantities of protein utilizing the principle of protein-dye binding. *Anal Biochem* 72:248-254.
5. Omura T & Sato R (1964) The carbon monoxide-binding pigment of liver microsomes. ii. solubilization, purification, and properties. *J Biol Chem* 239:2379-2385.
6. Li S, Ouellet H, Sherman DH, & Podust LM (2009) Analysis of transient and catalytic desosamine-binding pockets in cytochrome P-450 PikC from Streptomyces venezuelae. *J Biol Chem* 284(9):5723-5730.
7. Bai Z*, et al.* (2014) New chitosan-di(aryl carbamate)-(amide) prepared by dissolving chitosan in aqueous solution of organic acid, reacting, dissolving N-acylated chitosan in lithium chloride, adding phenyl isocyanate to N,N-dimethylacetamide, and reacting. Chinese patent CN104311700-A.
8. Du L*, et al.* (2016) Characterization of a Unique Pathway for 4-Cresol Catabolism Initiated by Phosphorylation in Corynebacterium glutamicum. *J Biol Chem* 291(12):6583-6594.
9. McKenna CE, Higa MT, Cheung NH, & McKenna M-C (1977) The facile dealkylation of phosphonic acid dialkyl esters by bromotrimethylsilane. *Tetrahedron Lett* 2:155-158.
10. Kenner GW & Williams NR (1955) A method of reducing phenols to aromatic hydrocarbons. *J Chem Soc*:522-525.
11. Romsted LS & Yoon CO (1993) Counterion affinity orders in aqueous micellar solutions of sodium decyl phosphate and sodium dodecyl sulfate determined by changes in sodium-23 NMR relaxation rates: a surprising dependence on head group charge. *J Am Chem Soc* 115(3):989-994.
12. Montgomery HAC & Turnbull JH (1958) 399. Phosphoramidic halides: phosphorylating agents derived from morpholine. *J Chem Soc* (0):1963-1967.
13. Ortiz de Montellano PR (2015) *Cytochrome P450: Structure, Mechanism, and Biochemistry* (Springer) 4th Ed.